described above and then were treated as described[46] with the following modifications: HCl treatment was for 9 min and BrdU detection was with FITC-conjugated anti-BrdU (3D4, BD Pharmingen) followed by alkaline phosphatase–conjugated anti-fluorescein.

Laser-capture microdissection and quantitative RT-PCR analysis. Lymph nodes were frozen in optimum cutting temperature compound as described above. Cryostat sections (7 μm in thickness) were affixed to glass foil slides for membrane-based laser microdissection (Leica), allowed to dry for 30 min at 20–25 °C, fixed for 1 min in 70% ethanol, washed for 30 s in distilled water, stained for 1 min with 0.6% (weight/volume) methyl green (Fluka), rinsed in distilled water, dehydrated by a graded ethanol series (70%, 95% and 100%) for 1 min each and allowed to air dry at 20–25 °C for 7–12 h. The following regions were isolated by laser-capture microdissection on a Leica AS LMD for each experiment: GC dark and light zones ($n = 40$–85), medullary cord regions ($n = 20$–40), primary follicles lacking GCs ($n = 30$–60), and T cell zones ($n = 15$–30). Microdissected regions were collected in the caps of 0.2-ml, thin-walled, RNase-free PCR tubes (Ambion). RNA was isolated with the RNeasy Micro Kit (Qiagen) with 'on-column' DNase treatment according to the manufacturer's instructions. First-strand cDNA was synthesized from RNA with Moloney murine leukemia virus reverse transcriptase (Promega) and random primers (Promega) according to the manufacturer's instructions. For quantitative PCR, 4–8% of the cDNA was placed in a final volume of 50 μl containing 1 × PCR Buffer II (Applied Biosystems, ABI), 5.5 mM $MgCl_2$ (ABI), 300 nM of each dNTP (PCR grade; Invitrogen), 1.25 units of AmpliTaq Gold DNA Polymerase (ABI) and primers and probes (Supplementary Table 4 online). Samples were analyzed on a Prism 7900HT (ABI) with the following thermal cycler conditions: 50 °C for 2 min and 95 °C for 10 min, and then 40 cycles of 95 °C for 15 s followed by 60 °C for 1 min. For quantification of the relative amount of starting mRNA in each sample, standard curves were generated for each primer-probe set by preparation of serial dilutions of a pooled mixture containing 4% of the cDNA prepared from each microdissected region, in duplicate wells, and analysis with SDS 2.1 software (ABI). The quantity of target gene determined for each sample was divided by the quantity of a housekeeping gene (*Gapd*), giving a relative ratio of mRNA expression.

Chemotaxis assays. Cell suspensions were prepared by mechanical disruption of spleens on 70-μm cell strainers (Fisher), and erythrocytes were lysed for 2 min at 20–25 °C with Tris-buffered NH_4Cl. Splenocytes were resuspended at a density of 1×10^7 cells per ml in RPMI 1640 medium containing L-glutamine, antibiotics, 10 mM HEPES buffer and 0.5% fatty acid–free BSA. Cells were resensitized for 30–60 min at 37 °C before being plated in Transwell inserts with a pore size of 5 μm and a diameter of 6.5 mm in 24-well plates (93421; Corning Costar). For these experiments, 100 μl cells (1×10^6) were added to the upper wells and 580 μl diluted chemokine was placed in the bottom wells at the indicated concentrations (Fig. 4b), and plates were incubated for 3 h at 37 °C in 5% CO_2. Migrated cells were counted by flow cytometry as described[47]. Duplicate wells were analyzed for each concentration of chemokine. Recombinant human SDF-1 was from Peprotech and recombinant mouse CXCL13 and CCL21 were from R&D Systems.

Note: Supplementary information is available on the Nature Immunology website.

ACKNOWLEDGMENTS

We thank D. Hargreaves, Y. Xu and M. Lesneski for technical assistance; C. Miller for training in laser-capture microdissection; J. Dietrich for surgical expertise; S. Jiang for cell sorting; D. Littman for *Cxcr4*$^{+/-}$ mice; M. Lipp for *Cxcr5*$^{-/-}$ mice; T. Roach for some Eμ-*Bcl2*-22 mice; F. Arenzana-Seisdedos for K15C antibody; J. Lin and other members of the Weiss Lab for Jurkat cells; the Werb lab for the use of equipment and supplies; the University of California San Francisco Diabetes Center for use of the ABI Prism 7900HT; S. Luther, T. Okada and G. Cinamon for advice and comments on the manuscript; and M. Matloubian, C. Lo and J. Cholfin for discussions. Work supported by Howard Hughes Medical Institute and grants AI40098 and AI45073 from the National Institutes of Health, and by predoctoral grants from Howard Hughes Medical Institute (C.D.C.A. and K.M.A.).

COMPETING INTERESTS STATEMENT

The authors declare that they have no competing financial interests.

Received 16 March; accepted 25 June 2004
Published online at http://www.nature.com/natureimmunology/

1. Röhlich, K. Beitrag zur Cytologie der Keimzentren der Lymphknoten. *Z. Mikrosk. Anat. Forsch.* **20**, 287–297 (1930).
2. MacLennan, I.C. Germinal centers. *Annu. Rev. Immunol.* **12**, 117–139 (1994).
3. Kelsoe, G. Life and death in germinal centers (redux). *Immunity* **4**, 107–111 (1996).
4. McHeyzer-Williams, M.G. & Ahmed, R. B cell memory and the long-lived plasma cell. *Curr. Opin. Immunol.* **11**, 172–179 (1999).
5. Berek, C., Berger, A. & Apel, M. Maturation of the immune response in germinal centers. *Cell* **67**, 1121–1129 (1991).
6. Liu, Y.J., Zhang, J., Lane, P.J., Chan, E.Y. & MacLennan, I.C. Sites of specific B cell activation in primary and secondary responses to T cell-dependent and T cell-independent antigens. *Eur. J. Immunol.* **21**, 2951–2962 (1991).
7. Koburg, E. in *Germinal Centers in Immune Responses.* (eds. Cottier, H., Odartchenko, N, Schindler, R. & Congdon, C.C.) 177–182 (Springer-Verlag, New York, University of Bern, Switzerland; 1966).
8. Koopman, G. *et al.* Adhesion of human B cells to follicular dendritic cells involves both the lymphocyte function-associated antigen 1/intercellular adhesion molecule 1 and very late antigen 4/vascular cell adhesion molecule 1 pathways. *J. Exp. Med.* **173**, 1297–1304 (1991).
9. Freedman, A.S. *et al.* Adhesion of human B cells to germinal centers in vitro involves VLA-4 and INCAM-110. *Science* **249**, 1030–1033 (1990).
10. Voigt, I. *et al.* CXCR5-deficient mice develop functional germinal centers in the splenic T cell zone. *Eur. J. Immunol.* **30**, 560–567 (2000).
11. Ansel, K.M. *et al.* A chemokine-driven positive feedback loop organizes lymphoid follicles. *Nature* **406**, 309–314 (2000).
12. Forster, R. *et al.* A putative chemokine receptor, BLR1, directs B cell migration to defined lymphoid organs and specific anatomic compartments of the spleen. *Cell* **87**, 1037–1047 (1996).
13. Roy, M.P., Kim, C.H. & Butcher, E.C. Cytokine control of memory B cell homing machinery. *J. Immunol.* **169**, 1676–1682 (2002).
14. Bowman, E.P. *et al.* Developmental switches in chemokine response profiles during B cell differentiation and maturation. *J. Exp. Med.* **191**, 1303–1318 (2000).
15. Bleul, C.C., Schultze, J.L. & Springer, T.A. B lymphocyte chemotaxis regulated in association with microanatomic localization, differentiation state, and B cell receptor engagement. *J. Exp. Med.* **187**, 753–762 (1998).
16. Forster, R. *et al.* Intracellular and surface expression of the HIV-1 coreceptor CXCR4/fusin on various leukocyte subsets: rapid internalization and recycling upon activation. *J. Immunol.* **160**, 1522–1531 (1998).
17. Casamayor-Palleja, M., Mondiere, P., Verschelde, C., Bella, C. & Defrance, T. BCR ligation reprograms B cells for migration to the T zone and B-cell follicle sequentially. *Blood* **99**, 1913–1921 (2002).
18. Estes, J.D. *et al.* Follicular dendritic cell-mediated up-regulation of CXCR4 expression on CD4 T cells and HIV pathogenesis. *J. Immunol.* **169**, 2313–2322 (2002).
19. Corcione, A. *et al.* Stromal cell-derived factor-1 as a chemoattractant for follicular center lymphoma B cells. *J. Natl. Cancer Inst.* **92**, 628–635 (2000).
20. Shinall, S.M., Gonzalez-Fernandez, M., Noelle, R.J. & Waldschmidt, T.J. Identification of murine germinal center B cell subsets defined by the expression of surface isotypes and differentiation antigens. *J. Immunol.* **164**, 5729–5738 (2000).
21. Maeda, K. *et al.* Murine follicular dendritic cells and low affinity Fc receptors for IgE (FcεRII). *J. Immunol.* **148**, 2340–2347 (1992).
22. Cyster, J.G. *et al.* Follicular stromal cells and lymphocyte homing to follicles. *Immunol. Rev.* **176**, 181–193 (2000).
23. Vonderheide, R.H. & Hunt, S.V. Does the availability of either B cells or CD4$^+$ cells limit germinal centre formation? *Immunology* **69**, 487–489 (1990).
24. Tamamura, H. *et al.* Enhancement of the T140-based pharmacophores leads to the development of more potent and bio-stable CXCR4 antagonists. *Org. Biomol. Chem.* **1**, 3663–3669 (2003).
25. Strasser, A. *et al.* Enforced BCL2 expression in B-lymphoid cells prolongs antibody responses and elicits autoimmune disease. *Proc. Natl. Acad. Sci. USA* **88**, 8661–8665 (1991).
26. Secord, E.A., Edington, J.M. & Thorbecke, G.J. The Eμ-bcl-2 transgene enhances antigen-induced germinal center formation in both BALB/c and SJL mice but causes age-dependent germinal center hyperplasia only in the lymphoma-prone SJL strain. *Am. J. Pathol.* **147**, 422–433 (1995).
27. Smith, K.G. *et al.* Bcl-2 transgene expression inhibits apoptosis in the germinal center and reveals differences in the selection of memory B cells and bone marrow antibody-forming cells. *J. Exp. Med.* **191**, 475–484 (2000).
28. Hargreaves, D.C. *et al.* A coordinated change in chemokine responsiveness guides plasma cell movements. *J. Exp. Med.* **194**, 45–56 (2001).
29. Okada, T. *et al.* Chemokine requirements for B cell entry to lymph nodes and Peyer's patches. *J. Exp. Med.* **196**, 65–75 (2002).
30. Krug, A. *et al.* IFN-producing cells respond to CXCR3 ligands in the presence of CXCL12 and secrete inflammatory chemokines upon activation. *J. Immunol.* **169**, 6079–6083 (2002).
31. Casamayor-Palleja, M. *et al.* Expression of macrophage inflammatory protein-3alpha, stromal cell-derived factor-1, and B-cell-attracting chemokine-1 identifies the tonsil crypt as an attractive site for B cells. *Blood* **97**, 3992–3994 (2001).

32. Amara, A. *et al.* Stromal cell-derived factor-1alpha associates with heparan sulfates through the first β-strand of the chemokine. *J. Biol. Chem.* **274**, 23916–23925 (1999).
33. Nieuwenhuis, P. & Opstelten, D. Functional anatomy of germinal centers. *Am. J. Anat.* **170**, 421–435 (1984).
34. Wehrli, N. *et al.* Changing responsiveness to chemokines allows medullary plasmablasts to leave lymph nodes. *Eur. J. Immunol.* **31**, 609–616 (2001).
35. Guinamard, R. *et al.* B cell antigen receptor engagement inhibits stromal cell-derived factor (SDF)-1α chemotaxis and promotes protein kinase C (PKC)-induced internalization of CXCR4. *J. Exp. Med.* **189**, 1461–1466 (1999).
36. Marchese, A. & Benovic, J.L. Agonist-promoted ubiquitination of the G protein-coupled receptor CXCR4 mediates lysosomal sorting. *J. Biol. Chem.* **276**, 45509–45512 (2001).
37. Balogh, P., Aydar, Y., Tew, J.G. & Szakal, A.K. Appearance and phenotype of murine follicular dendritic cells expressing VCAM-1. *Anat. Rec.* **268**, 160–168 (2002).
38. Egawa, T. *et al.* The earliest stages of B cell development require a chemokine stromal cell-derived factor/pre-B cell growth-stimulating factor. *Immunity* **15**, 323–334 (2001).
39. Ma, Q. *et al.* Impaired B-lymphopoiesis, myelopoiesis, and derailed cerebellar neuron migration in CXCR4- and SDF-1-deficient mice. *Proc. Natl. Acad. Sci. USA* **95**, 9448–9453 (1998).
40. Zou, Y.R., Kottmann, A.H., Kuroda, M., Taniuchi, I. & Littman, D.R. Function of the chemokine receptor CXCR4 in haematopoiesis and in cerebellar development. *Nature* **393**, 595–599 (1998).
41. Ara, T. *et al.* A role of CXC chemokine ligand 12/stromal cell-derived factor-1/pre-B cell growth stimulating factor and its receptor CXCR4 in fetal and adult T cell development *in vivo*. *J. Immunol.* **170**, 4649–4655 (2003).
42. Plotkin, J., Prockop, S.E., Lepique, A. & Petrie, H.T. Critical role for CXCR4 signaling in progenitor localization and T cell differentiation in the postnatal thymus. *J. Immunol.* **171**, 4521–4527 (2003).
43. Martin, C. *et al.* Chemokines acting via CXCR2 and CXCR4 control the release of neutrophils from the bone marrow and their return following senescence. *Immunity* **19**, 583–593 (2003).
44. Bleul, C.C., Fuhlbrigge, R.C., Casasnovas, J.M., Aiuti, A. & Springer, T.A. A highly efficacious lymphocyte chemoattractant, stromal cell-derived factor 1 (SDF-1). *J. Exp. Med.* **184**, 1101–1109 (1996).
45. Hernandez, P.A. *et al.* Mutations in the chemokine receptor gene CXCR4 are associated with WHIM syndrome, a combined immunodeficiency disease. *Nat. Genet.* **34**, 70–74 (2003).
46. Luther, S.A., Gulbranson-Judge, A., Acha-Orbea, H. & MacLennan, I.C. Viral superantigen drives extrafollicular and follicular B cell differentiation leading to virus-specific antibody production. *J. Exp. Med.* **185**, 551–562 (1997).
47. Ngo, V.N., Tang, H.L. & Cyster, J.G. Epstein-Barr virus-induced molecule 1 ligand chemokine is expressed by dendritic cells in lymphoid tissues and strongly attracts naive T cells and activated B cells. *J. Exp. Med.* **188**, 181–191 (1998).
48. Cinamon, G. *et al.* Sphingosine 1-phosphate receptor 1 promotes B cell localization in the splenic marginal zone. *Nat. Immunol.* **5**, 713–720 (2004).

Chemokine receptor expression in EBV-associated lymphoproliferation in hu/SCID mice: implications for CXCL12/CXCR4 axis in lymphoma generation

Erich Piovan, Valeria Tosello, Stefano Indraccolo, Anna Cabrelle, Ilenia Baesso, Livio Trentin, Rita Zamarchi, Hirokazu Tamamura, Nobutaka Fujii, Gianpietro Semenzato, Luigi Chieco-Bianchi, and Alberto Amadori

The mechanisms by which intraperitoneal injection of peripheral blood mononuclear cells (PBMCs) from Epstein-Barr virus (EBV)–seropositive donors into severe combined immunodeficient (SCID) mice gives rise to lymphomas (hu/SCID tumors) are far from clear. This study addressed whether chemokine receptors and their ligands could be implicated in this experimental model. CXCR4 was found to be highly expressed in hu/SCID tumors; surface expression of CXCR4 was prevalently limited to a tumor cell subset poorly expressing CD23, whereas the CXCR4 ligand, CXCL12, was predominantly expressed by the tumor subpopulation expressing CD23. In vitro inhibition of this autocrine/paracrine CXCL12/CXCR4 axis significantly inhibited lymphoma proliferation and survival. Furthermore, CXCL12 was expressed in cells recovered from the mouse peritoneal cavity early after PBMC transfer as well as by EBV-transformed B cells but not by resting or activated B lymphocytes; also, lymphoma development was associated with a dramatic increase in the levels of murine CXCL12 present in the peritoneal cavity. Finally, antagonizing the CXCL12/CXCR4 axis in vivo strongly counteracted lymphoma development. These studies demonstrate that CXCL12 expression may be associated with EBV infection and suggest that the CXCR4/CXCL12 axis may participate in the EBV-associated lymphomagenesis process in immunodeficient hosts. (Blood. 2005;105:931-939)

Introduction

Epstein-Barr virus (EBV) is implicated in the pathogenesis of at least 3 malignant disorders of B cells: Burkitt lymphoma, Hodgkin disease, and B-cell lymphoproliferative disease (BLPD) seen in immunosuppressed allograft recipients.[1] The severe combined immunodeficient (SCID) mouse, which lacks functional B and T cells,[2] is a suitable animal model for the study of EBV-associated lymphoproliferation.[3,4] SCID mice injected intraperitoneally with peripheral blood mononuclear cells (PBMCs) from EBV-positive donors develop EBV-positive human B-cell lymphomas (hu/SCID tumors),[4] which display a surface phenotype closely resembling that seen in BLPD with low expression of EBV latent proteins and presenting a mixture of lymphoblastoid and plasmacytoid cells.[5] The events occurring in the peritoneal cavity of PBMC-injected mice are very complex[6] and entail T-cell activation and massive cytokine production, both of which favor the expansion of B lymphocytes, including EBV-positive B-cell precursors. In this regard, we showed that the presence of T lymphocytes within the cellular inoculum is necessary for lymphoma development,[7] and treatment of PBMC-injected mice with cyclosporin A paradoxically counteracts tumor generation.[7,8] Recently, we also demonstrated that no EBV reactivation occurs during the lymphomagenesis process, and tumor masses originate from the expansion of the very few latently infected B lymphocytes present in the inoculum.[9]

Hu/SCID tumors consist of multiple masses at the hepatic hilus, lower splanchnic region, and within the mesenteric tissue,[7] the privileged sites of primary and/or metastatic localization being peritoneum, liver, and lymph nodes. Interestingly, all these organs have been reported to produce high levels of the CXCR4 ligand (CXCL12, previously called stromal cell–derived factor-1 [SDF-1])[10,11]; indeed, no tumor development occurs when PBMCs from EBV-positive donors are injected by other routes,[4] suggesting a critical role of the peritoneal environment for lymphomagenesis. In this regard, it has recently been shown that CXCL12, produced by mesothelial cells lining the peritoneum, is involved in the persistence of peritoneal B lymphocytes in mice[11]; indeed, CXCR4 is expressed on mature B cells.[12]

In view of these observations, we addressed whether chemokine receptors and their ligands could be implicated in EBV-mediated lymphomagenesis in this experimental model. Aims of our study were (1) to define the chemokine receptor expression profile of lymphoblastoid cell lines (LCLs) and hu/SCID tumors; (2) to assess whether chemokines were differentially expressed following cellular transformation by EBV; and (3) to evaluate whether any of the latter could contribute to the outgrowth of EBV-transformed B cells in the immunocompromised host.

From the Department of Oncology and Surgical Sciences, Oncology Section, University of Padua, Italy; Istituto Nazionale per la Ricerca sul Cancro-IST, Genua, Italy; Department of Clinical and Experimental Medicine, Clinical Immunology Branch, University of Padua, Italy; Graduate School of Pharmaceutical Sciences, Kyoto University, Japan; Azienda Ospedaliera Padova, Padua, Italy; and Venetian Institute for Molecular Medicine, Padua, Italy.

Submitted March 2, 2004; accepted September 16, 2004. Prepublished online as *Blood* First Edition Paper, September 28, 2004; DOI 10.1182/blood-2004-03-0799.

Supported in part by grants from Ministero dell'Instruzione, dell' Universitá e della Ricerca (MIUR; FIRB and PRIN and MUIR 60%); Istituto Superiore di Sanità (AIDS Project); Italian Association for Research on Cancer (AIRC) and Italian Foundation for Research on Cancer (FIRC); and Padua University grants. V.T. is a recipient of an AIRC fellowship.

Reprints: Erich Piovan, Department of Oncology and Surgical Sciences, Oncology Section, University of Padua, via Gattamelata 64, Padua, I-35128, Italy; e-mail: erich.piovan@unipd.it.

The publication costs of this article were defrayed in part by page charge payment. Therefore, and solely to indicate this fact, this article is hereby marked "advertisement" in accordance with 18 U.S.C. section 1734.

We report here that lymphoma development in PBMC-injected SCID mice is associated with down-regulated expression by EBV-transformed B cells of the chemokine receptors CCR6, CCR7, and CXCR5, while CXCR3 and CXCR4 are expressed at moderately high levels. We show that most hu/SCID tumors express functional CXCR4 receptors and that CXCL12 affects several biologic responses, including migration, adhesion, proliferation, and invasion. In adjunct, we demonstrate that CXCL12 expression may be related to immortalization of B cells by EBV. We also demonstrate that the hu/SCID tumor subset poorly expressing CD23 expresses functional CXCR4; meanwhile, the tumor subset expressing CD23 is the main producer of CXCL12, suggesting a potential chemotactic loop between these 2 cell populations. Finally, antagonizing the CXCR4/CXCL12 axis through the use of a neutralizing anti-CXCL12 antibody (Ab) or a CXCR4 antagonist was able to counteract lymphoma growth. Because CXCR4 is expressed in the human counterpart of hu/SCID tumors,[13,14] these observations may be relevant to the human setting and open new avenues to therapeutic approaches in B-cell non-Hodgkin lymphomas.

Materials and methods

Isolation of PBMCs and B-cell purification

PBMCs were isolated by Ficoll-Hypaque (Pharmacia Biotech, Uppsala, Sweden) gradient centrifugation as reported elsewhere,[15] washed 4 times with RPMI medium, counted, and used as such for establishment of LCLs and inoculation of SCID mice or separated further. LCLs were generated and maintained as previously reported.[9] Purified B cells were obtained from PBMCs by positive selection using magnetic microbeads (Miltenyi Biotec, Bergisch Gladbach, Germany) according to manufacturer's recommendations.[9] Recovered B cells were of 95% to 98% purity, as determined by flow cytometric analysis. B-cell cultures were set up as previously described.[16]

Generation of human B-cell tumors in SCID mice

SCID mice were purchased from Charles River (Wilmington, MA) and maintained in our animal facilities under pathogen-free conditions. Procedures involving animals and their care conformed with institutional guidelines that comply with national and international laws and policies (European Community EEC Council Directive 86/609, OJ L 358, December 12, 1987). Groups of 7- to 9-week-old SCID mice were injected intraperitoneally with 70×10^6 to 100×10^6 unfractionated PBMCs, observed daily for signs of illness, and killed by cervical dislocation when they became sick. Tumors and other tissues of interest were processed as previously described.[9]

In another set of experiments, hu/SCID tumor cell suspensions were briefly expanded in vitro before being injected intraperitoneally (2×10^6) into SCID mice. Groups of 5 to 8 hu/SCID lymphoma-injected SCID mice were treated with intraperitoneal injections of a polyclonal goat anti-CXCL12 Ab (kindly provided by Prof Robert M. Strieter, UCLA, Los Angeles, CA; 50 μL per mouse per injection); 500 μL of this Ab is sufficient to neutralize 1 μg of either human or murine CXCL12 in leukocyte chemotaxis assays.[17] As controls, we used heat-inactivated goat preimmune serum and phosphate-buffered saline (PBS). The animals were treated every day for 3 weeks starting from the day after tumor injection, and the effects of anti-CXCL12 Ab treatment on lymphoma development were assessed by monitoring survival and histologic examination for evidence of tumor. In other groups of animals (6 to 8 mice) the day before transplantation of lymphoma cells, Alzet pumps (duration 14 days; model 1002, ALZA, Mountain View, CA) containing 50 to 80 mg/mL of the CXCR4-specific antagonist 4F-benzoyl-TN14003[18] or vehicle were implanted subcutaneously. On day 13, the Alzet pumps were replaced with pumps containing the same amounts of peptide or vehicle.

FACS analysis

The following mouse monoclonal antibodies (mAbs) were used: phycoerythrin (PE)–labeled mAb against CCR1 (IgG2a), CCR2 (IgG2a), CCR4 (IgG1), CCR6 (IgG2b), CXCR4 (IgG2b), CXCR5 (IgG2a) (all from R&D Systems, Minneapolis, MN), and CD23 (IgG3; Immunotech, Marseille, France); and fluorescein isothiocyanate (FITC)–labeled mAb to CCR3 (IgG2a), CCR5 (IgG2a), CCR7 (IgG1), CXCR1 (IgG2a), CXCR2 (IgG2a), CXCR3 (IgG1) (all from R&D Systems), and CD23 (IgG1; Becton Dickinson, Mountain View, CA). Irrelevant conjugated mouse Abs of each isotype (Becton Dickinson) were used to establish specificity of staining. The following Abs also were used: rabbit anti-CXCL12 Ab (PeproTech, London, United Kingdom), irrelevant rabbit immunoglobulin G (IgG) (PeproTech), and Alexa 488–labeled goat antirabbit Ab (Molecular Probes, Leiden, The Netherlands). Results were expressed as percent of the cells expressing the relevant marker.

Intracellular expression of CXCL12 in LCLs and hu/SCID tumor cells was detected by flow cytometry as previously described.[19]

Isolation of RNA and RT-PCR

Total RNA was isolated using the RNeasy mini kit (QIAGEN, Hilden, Germany), primed (0.5 to 1 μg) with random hexamers (Promega, Madison, WI), and reverse transcribed. Complementary DNA fragments from the reverse transcriptase (RT) reaction mixture were subjected to polymerase chain reaction (PCR) amplification using AmpliTaq Gold polymerase (Applied Biosystems, Foster City, CA) for 35 to 45 cycles (95°C for 45 seconds, 60°C for 45 seconds, 72°C for 1 minute). The following primers were used: human CXCL12: forward, 5′-ATGAACGCCAAGGTCGTGGTCG-3′, reverse (SDF-1α), 5′-AAGTCCTTTTTGGCTGTTGTGC-3′, or reverse (SDF-1β) 5′-TGACCCTCTCACATCTTGAACC-3′ [20]; human CXCR4: forward, 5′-GGGGATCAGTATATACACTTCAG-3′, reverse, 5′-AGACGCCAACATAGACCAC-3′; mouse CXCL12: forward, 5′-CACCTCGGTGTCCTCTTG-3′, reverse, 5′-GGTCAATGCACACTTGTCTG-3′. For the control of RNA and cDNA preparations, we used RT-PCR for β-actin as previously reported.[21] Amplified products were analyzed on a 1.8% agarose electrophoresis gel and visualized under UV rays after ethidium bromide staining.

In vitro adhesion assays

Adhesion of hu/SCID tumor cells to human umbilical vein endothelial cells (HUVECs) and fibronectin was assayed as previously described,[22,23] with minor modifications. Briefly, hu/SCID tumor cells (1×10^5) were labeled before the assay with the fluorescent dye calcein acetoxymethyl ester (calcein-AM; Molecular Probes) and were subsequently added for 30 to 60 minutes to 96-well culture plates covered by HUVECs, bovine serum albumin (BSA; 40 μg/mL; Sigma, St Louis, MO), or fibronectin (10 μg/mL). After the incubation period, the nonadherent cells were removed by vigorously washing the wells with RPMI 1640 medium (Life Technologies, Grand Island, NY) 3 times. Adherent cells were collected and counted by flow cytometry. A gate was set up using the calcein labeling of the lymphoma cells to exclude HUVECs from the counts. Results were expressed as percentage of adherent cells (ie, number of adherent cells per number of input cells).

For inhibition studies, hu/SCID tumor cells were preincubated with a neutralizing anti-CXCL12 Ab (1:100) or 1 μM TC14012, a CXCR4-specific inhibitor,[24] for 30 minutes at 37°C before being plated in HUVEC- or fibronectin-coated wells.

Chemotaxis and chemoinvasion assay

Migration and invasion were assayed in modified Boyden chambers (Neuro Probe, Gaithersburg, MD) using 13-mm polycarbonate filters of 8-μm pore size as previously described.[25,26] Membranes were uncoated for chemotaxis or coated with 25 μg Matrigel (Becton Dickinson) for invasion assays. The lower compartments were filled with RPMI supplemented with 0.1% BSA with or without CXCL12 (100 to 200 ng/mL). Hu/SCID tumor cells were preincubated for 30 minutes at 37°C in the presence of 1 μM TC14012, anti-CXCL12 Ab, or in control conditions (RPMI–0.1% BSA) and subsequently loaded (3×10^5) onto the upper compartments of the modified

Boyden chambers. After incubation of 2 hours (chemotaxis) or 24 hours (chemoinvasion), the contents of the lower compartments were collected and counted after fixation and staining with crystal violet.

Actin polymerization

To evaluate the effect of CXCL12 on cytoskeleton rearrangement of different tumor subsets, freshly isolated hu/SCID lymphoma cells were labeled with PE-conjugated anti-CD23 mAb at 4°C for 30 minutes. Cells were washed and incubated at 37°C in RPMI medium before assessing cytoskeleton rearrangement. Actin polymerization experiments were performed as previously described.[11]

Proliferation and survival assays

For proliferation and survival studies evaluating the role of endogenous CXCL12, freshly isolated hu/SCID tumor cell suspensions treated with or without anti-CXCL12 Abs (1:20) or TC14012 (50 to 100 μM) were pulsed for 48 hours with 1 μCi [37 Bq] [methyl-^{3}H]thymidine (Amersham, Arlington Heights, IL) or labeled with FITC-conjugated annexin V (PharMingen, BD Biosciences, San Diego, CA) plus propidium iodide (PI; Molecular Probes).[19] Subsequently, thymidine incorporation was evaluated on a scintillation β-plate counter, or the percentage of cells undergoing apoptosis was determined by flow cytometry. Annexin V–positive PI-negative and annexin V–positive PI-positive cells correspond to apoptotic and necrotic cells, respectively.

Confocal microscopy

Confocal microscopic analysis was executed as previously described.[27] Cells were stained with the following primary Abs: mouse anti-CXCR4 mAb (R&D Systems) and rabbit anti–human CXCL12 Ab (PeproTech), while the secondary Abs used were Alexa 594–conjugated anti–mouse Ab (Molecular Probes; red signal) and an Alexa 488–conjugated antirabbit Ab (Molecular Probes; green signal).

Murine CXCL12 ELISA

Peritoneal washings were executed as previously described.[9] For each time point considered, 3 to 5 mice were killed and the liquid obtained from the peritoneal washings of each time point was pooled together. These pools were concentrated 50 times with Centriplus Centrifugal Filter Devices (YM-3; Millipore, Billerica, MA) to obtain a final volume of 300 to 500 μL. The quantity of murine CXCL12 present in the peritoneal washings was then determined using an antibody sandwich enzyme-linked immunosorbent assay (ELISA) (R&D Systems) with a sensibility of more than 44 pg/mL.

Statistical analysis

Results were expressed as mean value ± SD. Statistical analyses of the in vitro data were performed using the nonparametric Mann-Whitney test; in in vivo experiments, Kaplan-Meier survival curves were analyzed with the Mantel-Haenszel test.

Results

EBV transformation of B cells in vitro (LCLs) and in vivo (hu/SCID tumors) is associated with modulation of chemokine receptor expression

The chemokine receptor expression profile of EBV-transformed B cells has not been as yet extensively addressed. Using a panel of mAbs directed against CCR1, CCR2, CCR3, CCR4, CCR5, CCR6, CCR7, CXCR1, CXCR2, CXCR3, CXCR4, and CXCR5, we compared the chemokine receptor expression profile in freshly isolated B lymphocytes, in vitro EBV-immortalized LCL cells, and in vivo–generated hu/SCID tumors. Data are summarized in Figure 1. Circulating B cells expressed CCR6, CCR7, CXCR3, CXCR4, and CXCR5 (Figure 1, circles); very rarely, CCR1, CCR4, CCR5, and CXCR2 were expressed at low levels (data not shown). In contrast, EBV-immortalized LCL cells expressed CCR7, CXCR3, and CXCR4 at a lower level ($P < .05$), with CCR6 and CXCR5 being frequently undetectable (Figure 1, squares); rarely, CCR1, CCR3, and CCR4 were positive at low levels (data not shown). Hu/SCID tumors presented a mixed chemokine receptor expression profile (Figure 1, triangles), with CXCR3 and CXCR4 being substantially expressed, while CCR6, CCR7, and CXCR5 were significantly more weakly expressed compared with freshly isolated B lymphocytes ($P < .05$); rarely, CCR1, CCR2, and CCR4 were positive at low levels (data not shown). In general, a lower percent expression of chemokine receptors was also paralleled by a sizable reduction in mean fluorescence intensity (MFI) of the cells (data not shown). Altogether, these data demonstrate that EBV transformation in vitro is associated with a significant down-regulation of the expression of all chemokine receptors studied (CCR6, CCR7, CXCR3, CXCR4, and CXCR5); on the contrary, EBV-positive hu/SCID tumors generated after PBMC transfer into SCID mice continue to express substantial levels of CXCR3 and CXCR4, comparable to those present in freshly isolated B cells, though down-modulating CCR6, CCR7, and CXCR5.

CXCR4 is functional and is predominantly expressed by a CD23^{low} hu/SCID tumor cell population

The functionality of the chemokine receptors expressed on hu/SCID tumor cells was evaluated by a chemotaxis assay. In most cases CXCL12 gave the greatest chemotactic response (data not shown), and because tumors in our experimental model consist of multiple peritoneal masses with frequent involvement of liver, spleen, and abdominal lymph nodes, sites known to produce high levels of CXCL12,[10] subsequent experiments focused on the CXCL12/CXCR4 axis. As shown in Figure 2A, chemotaxis to

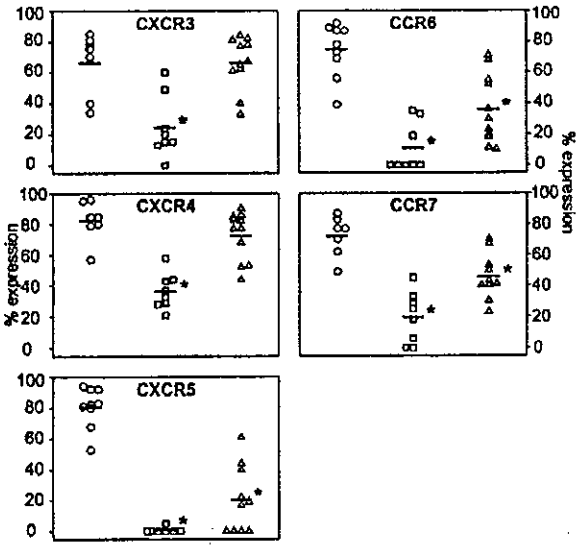

Figure 1. Modulation of chemokine receptor expression in EBV-transformed B cells in vitro (LCLs) and in vivo (hu/SCID tumors). Flow cytometric analysis for CCR6, CCR7, CXCR3, CXCR4, and CXCR5 expression on B lymphocytes (○), LCL cells (□), and freshly isolated hu/SCID tumor cells (△). Each point shows the percentage of cells expressing the indicated chemokine receptor. Horizontal bars represent the mean value of each group; the asterisks denote a significant difference compared with B cells ($P < .05$).

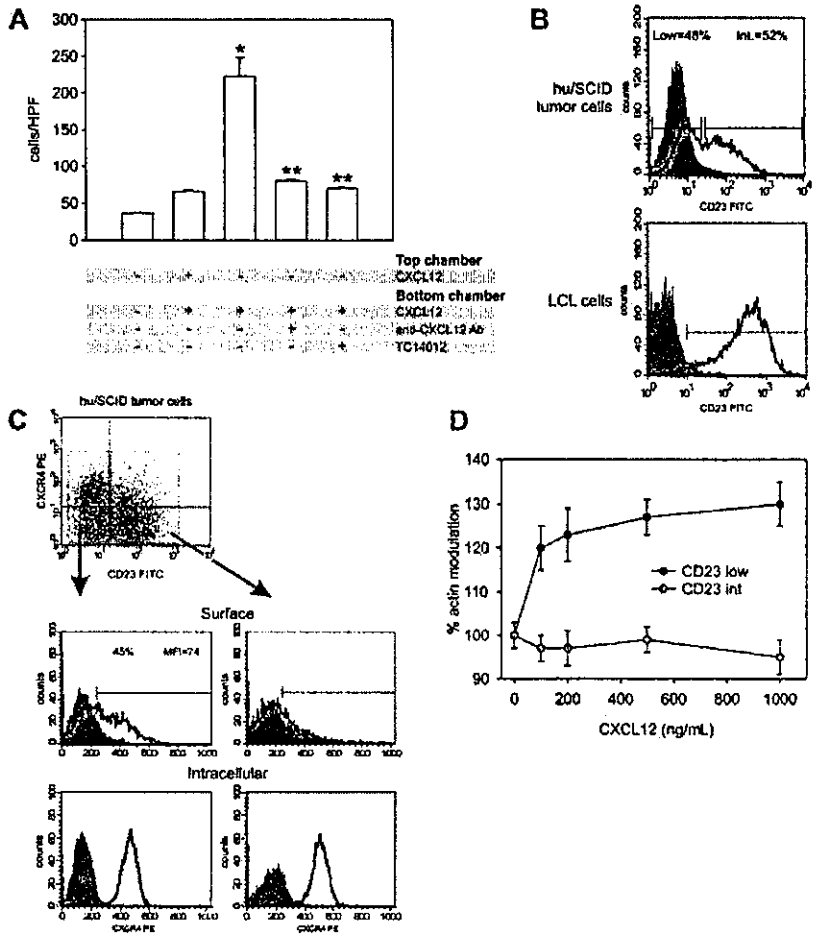

Figure 2. CXCR4 is functional, and its surface expression segregates with B-cell phenotype in hu/SCID tumor cells. (A) Effect of CXCL12 on migration of hu/SCID lymphoma cells. Lymphoma cells were added to the chemotaxis chamber in the presence (+) or absence (−) of the following reagents: 100 ng/mL CXCL12 (SDF-1α), neutralizing anti-CXCL12 Abs (1:100), and TC14012 (1 and 5 μM). Migrated cells were recovered from the lower chamber after 2 hours at 37°C and counted. Results are the mean of 2 separate experiments executed in triplicate (± SD). The single asterisk denotes a significant difference compared with untreated cells ($P < .05$); 2 asterisks denote a significant inhibition by TC14012 or anti-CXCL12 Abs of the chemotactic properties of CXCL12-stimulated cells ($P < .05$). (B) Tumor cells were stained with the FITC-conjugated anti-CD23 mAb and the PE-conjugated anti-CXCR4 mAb before being analyzed by cytofluorimetry. The fluorograms represent the expression pattern of CD23 in a representative hu/SCID tumor sample (top) and LCL cells (bottom). (C) The expression of surface and intracellular CXCR4 (upper and lower panels, respectively) in the $CD23^{low}$ (left diagrams) and $CD23^{int}$ (right diagrams) tumor cell subsets is shown. A representative experiment of 3 consecutive experiments is shown. (D) Effect of CXCL12 on actin polymerization in the 2 hu/SCID lymphoma cell subsets. Lymphoma cells were labeled with PE-conjugated anti-CD23 Ab and tested by flow cytometry for CXCL12-induced cytoskeleton rearrangement. Results (mean ± SD from 2 experiments) show the kinetics of actin polymerization following addition of different concentrations of CXCL12; 100% corresponds to the baseline level.

CXCL12 could be significantly blocked by pretreatment of cells with neutralizing Abs to CXCL12 and the CXCR4 antagonist TC14012. Further, no significant increase of migration was observed with a uniform distribution of CXCL12, indicating that this is a gradient-dependent chemotactic response. It has been reported that hu/SCID tumors are composed of 2 phenotypically distinct B-cell subsets: $CD23^{low}$ (and $CD38^{high}$ [$CD38^{hi}$]) and $CD23^{intermediate}$ ([$CD23^{int}$] and $CD38^{(int)}$), demonstrated to harbor a different EBV gene expression profile[5]; on the other hand, LCL cells have been reported to be homogenously $CD23^{hi}CD38^{int/low}$ and only show a reduced CD23 expression when transferred into SCID mice.[5,28] We thus investigated whether CXCR4 expression on hu/SCID tumor cells was segregated with the B-cell phenotype. To analyze the coexpression of membrane CXCR4 and CD23 on hu/SCID tumors, the tumor cells were examined cytometrically after staining with FITC anti-CD23 and PE anti-CXCR4 mAbs. As shown in Figure 2B (upper panel), in agreement with previously published data,[5] within hu/SCID tumor cells 2 cell subpopulations were discernable on the basis of CD23 expression, one $CD23^{low}$ and one $CD23^{int}$; this was not the case for LCLs, where virtually all cells showed high CD23 expression (Figure 2B, lower panel). Further, a clear segregation in CXCR4 expression was observed in the 2 hu/SCID tumor cell subpopulations (Figure 2C), with CXCR4 surface expression being predominantly confined to the $CD23^{low}$ subset (Figure 2C, top left panel). On the other hand, both tumor cell subsets expressed consistent levels of internal CXCR4 (Figure 2C). To determine the functional relevance of the generation of the 2 cell subsets, we investigated F-actin modulation following incubation with increasing concentrations of CXCL12. As shown in Figure 2D, a significant increase in F-actin polymerization could be observed only in the $CD23^{low}$ tumor subset, suggesting that this subset is the main responder to CXCL12.

The CXCR4 ligand, CXCL12, is expressed by LCLs and a CD23-expressing hu/SCID tumor cell population but not resting or activated B cells

EBV-transformed B lymphocytes have a propensity to produce autocrine factors for their own growth and survival.[29,30] We evaluated by both RT-PCR and fluorescence-activated cell sorter (FACS) analysis whether LCLs and hu/SCID tumors expressed the CXCR4 ligand, CXCL12, thus possibly activating an autocrine loop; indeed, this has not been investigated so far. As shown in Figure 3A, all LCLs (lanes 1 to 5) and hu/SCID tumor cells (lanes 6 to 10) tested expressed mRNA for SDF-1α/CXCL12 and most also expressed SDF-1β/CXCL12 (data not shown), with the α isoform being the predominant transcript in most cases. To investigate whether the expression of CXCL12 by LCLs and hu/SCID tumor cells was simply associated to the activation state of these cells or more strictly linked to EBV transformation, B cells were purified and stimulated in vitro with anti-CD40 mAb and interleukin-4 (IL-4) for 3 to 5 days. RT-PCR analysis of these samples disclosed that no specific transcripts for SDF-1α/CXCL12 or SDF-1β/CXCL12 could be evidenced in both freshly isolated (Figure 3A,

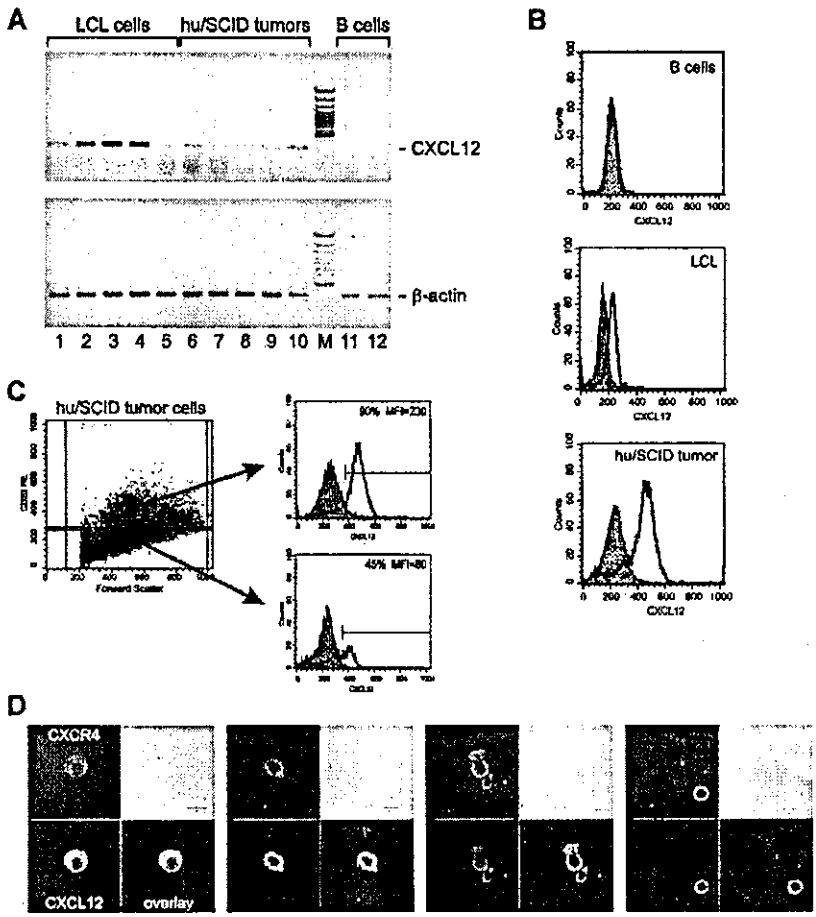

Figure 3. CXCL12 expression in EBV-transformed B cells and its segregation with B-cell phenotype. (A) The expression of CXCL12 and β-actin in LCL cells and hu/SCID tumor cells was evaluated by RT-PCR. Representative results from 5 LCLs and 5 hu/SCID tumors are shown. Lane M corresponds to 50-bp molecular weight marker. Lanes 12 and 13 correspond to a representative case of purified resting B cells and to the same B cells after 48 hours of in vitro stimulation with anti-CD40/IL-4, respectively. (B-C) The intracellular expression of CXCL12 in LCL cells and hu/SCID tumor cells was evaluated by cytofluorimetric analysis. (B) The fluorograms (from top to bottom) show normal B cells not expressing CXCL12, LCL cells, and hu/SCID tumor cells. (C) The expression of CXCL12 in the $CD23^{low}$ (lower right) and $CD23^{int}$ (upper right) tumor cell subsets is shown. A representative experiment of 3 consecutive experiments is shown. (D) Confocal microscopic analysis evaluating the coexpression of surface CXCR4 and intracellular CXCL12 in hu/SCID tumors. Cells were fixed, stained with anti-CXCR4 Ab, and subsequently permeabilized before incubation with anti-CXCL12 Ab. The signal for CXCR4 is shown in red, while the CXCL12 signal is in green. Areas of colocalization are shown in yellow.

lane 11 of each panel) and in vitro–activated B cells (Figure 3A, lane 12 of each panel), thus showing that CXCL12 expression was in some way associated with EBV immortalization. The expression of CXCL12 in EBV-transformed B cells was also confirmed at the protein level by cytofluorimetric analysis of both LCLs and hu/SCID tumors (Figure 3B); interestingly, CXCL12 was shown to be preferentially produced by the CD23-expressing (LCL-like) subset of hu/SCID tumors (Figure 3C). To better document the segregation of CXCR4 and CXCL12 expression in hu/SCID tumors, we executed confocal microscopy analysis at the single cell level after staining the cells for surface CXCR4 and intracellular CXCL12. As shown in Figure 3D, on the whole, cells expressing high levels of surface CXCR4 (red signal) expressed much more weakly CXCL12 (green signal) compared with the cell population expressing CXCR4 weakly or not at all.

In vitro CXCL12 neutralization inhibits hu/SCID lymphoma cell proliferation and survival

We showed thus far that hu/SCID tumors express CXCL12 and that they can efficiently respond to exogenous CXCL12. We thus set out to investigate the possible functional role of endogenous CXCL12 on hu/SCID cell biology. We first investigated whether CXCL12 neutralization by the use of anti-CXCL12 neutralizing Abs or the use of a recently described specific blocking agent for CXCR4,[24] such as TC14012, affected lymphoma growth in vitro. Indeed, as shown in Figure 4A, treatment of ex vivo–obtained lymphoma cells for 2 days with neutralizing anti-CXCL12 Abs (1:20 dilution) or TC14012 (50 to 100 μM) significantly reduced lymphoma cell proliferation ($P < .05$). On the other hand, the goat preimmune serum used as control at the same dilution did not significantly alter lymphoma proliferation (Figure 4A). We next tested the effect of

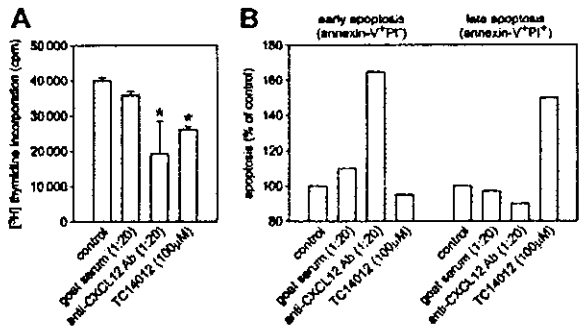

Figure 4. Effect of in vitro neutralization of CXCL12 and CXCR4 on hu/SCID lymphoma cell proliferation and survival. (A) Ex vivo–obtained hu/SCID lymphoma cells were cultured for 48 hours with or without TC14012 (50 to 100 μM), neutralizing anti-CXCL12 Abs (1:20), or appropriate controls. Each result is representative of the mean counts per minute (cpm) ± SD of triplicate wells after a 48-hour pulse with [methyl-^{3}H]thymidine. This analysis is representative of 3 separate experiments with different tumors with similar results; the single asterisk denotes a significant difference compared with untreated cells ($P < .05$). (B) Ex vivo–obtained hu/SCID lymphoma cells were cultured for 48 hours with or without TC14012 (50 to 100 μM), neutralizing anti-CXCL12 Abs (1:20), or appropriate controls. Cells were then harvested and labeled with PI and FITC-conjugated annexin V before being analyzed by flow cytometry. Data are shown as the mean percent change relative to control. One representative experiment of 3 performed is shown.

blocking the endogenous CXCL12 on apoptosis of hu/SCID lymphoma cells. To this end, ex vivo–obtained lymphoma cells were treated for 2 days with neutralizing anti-CXCL12 Abs (1:20 dilution) or TC14012 (50 to 100 μM) and then analyzed by flow cytometry after staining with FITC-conjugated annexin V and PI. Treatment of cells with either anti-CXCL12 Abs or TC14012 determined a significant increase in annexin V–positive cells (data not shown). However, a difference seemed to emerge in their mode of action, because the neutralizing anti-CXCL12 Abs determined mainly an increase in early apoptosis (annexin V–positive PI-negative), while the CXCR4 antagonist acted mainly on late apoptosis (annexin V–positive PI-positive) (Figure 4C). Notably, the concentrations of the neutralizing anti-CXCL12 Abs (1:100 dilution) or TC14012 (1 to 5 μM) used in functional assays such as chemotaxis, adhesion, or chemoinvasion did not affect either the proliferation or survival of lymphoma cells (data not shown). On the whole, these data suggest that survival and proliferation of hu/SCID tumors are in part mediated by CXCL12/CXCR4 interactions and autocrine secretion of CXCL12.

CXCL12 stimulates the adhesive and invasive properties of hu/SCID tumor cells

CXCL12 has been reported to regulate the function of several integrins on normal human hematopoietic cells[31]; we thus investigated whether CXCL12 also regulated integrin activity in hu/SCID tumor cells. As shown in Figure 5A, CXCL12 consistently increased the adhesion of hu/SCID tumor cells to both fibronectin (Figure 5A, middle panel) and HUVECs (Figure 5A, right panel), whereas it did not affect their adhesion to BSA (Figure 5A, left panel).

Because tumor cell invasion is one of the major characteristics of malignant cells, we evaluated this feature using a chemoinvasion Matrigel assay. As shown in Figure 5B, the invasive capability of hu/SCID tumors was increased in the presence of a CXCL12 gradient (Figure 5B, open columns). In addition, TC14012 significantly inhibited both the adhesive and invasive properties of these cells (Figure 5, gray columns), thus indicating that the invasion-promoting effect of CXCL12 was a specific phenomenon; similar results were obtained when neutralizing anti-CXCL12 Abs were used (data not shown).

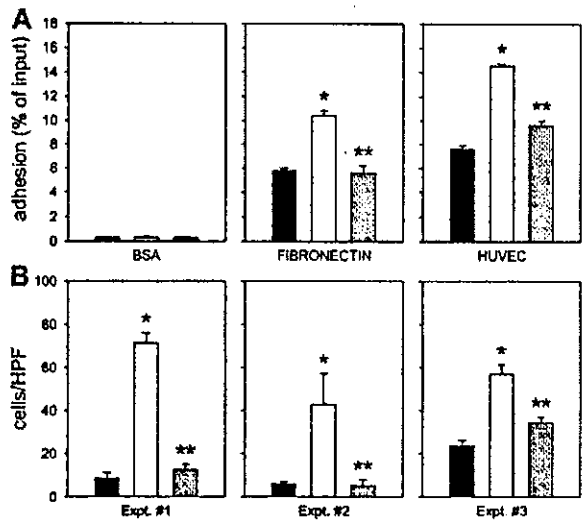

Figure 5. Effect of CXCL12 on the adhesive and invasive properties of hu/SCID tumor cells. (A) Effect of CXCL12 on adhesion of hu/SCID tumor cells to fibronectin and endothelial cells. The panels from left to right represent adhesion of hu/SCID tumor cells to bovine serum albumin (BSA), fibronectin, and HUVECs. Unstimulated cells are shown as black bars; open and gray bars represent hu/SCID tumor cells stimulated with CXCL12/SDF-1α (200 ng/mL) in the absence and in the presence, respectively, of the CXCR4 antagonist TC14012. Data are shown as mean ± SEM of 2 consecutive experiments; the single asterisk denotes a significant difference compared with untreated cells ($P < .05$); 2 asterisks denote a significant inhibition by TC14012 of the adhesive properties of CXCL12-stimulated cells ($P < .05$). (B) Cells invading the Matrigel were collected from the lower compartments and counted as detailed in "Materials and methods"; results are expressed as number of cells per high power field (HPF) and represent mean values ± SEM of 3 replicate determinations for each tumor. Hu/SCID lymphoma cells showed significant invasion through Matrigel toward a CXCL12 gradient (open columns); this phenomenon was inhibited by treating the cells with TC14012 (gray columns). The single asterisk denotes a significant difference ($P < .05$) compared with unstimulated cells; 2 asterisks denote a significant inhibition by TC14012 of the invasive properties of CXCL12-stimulated cells ($P < .05$). Results obtained in 3 different hu/SCID tumor masses representative of 4 consecutive experiments are shown.

CXCL12 is expressed in vivo during the early phases of EBV-mediated lymphomagenesis, and its neutralization inhibits tumor growth in vivo

We finally directly addressed the possible relevance of the CXCL12/CXCR4 axis in the lymphomagenesis process of this experimental model. To this end, we first wondered whether CXCL12 and CXCR4 were indeed expressed in the mouse peritoneal microenvironment. Thus, cells were recovered from the peritoneal cavity of SCID mice at 4, 8, and 16 days following intraperitoneal transfer of PBMCs from EBV-positive donors, and the expression of human and murine CXCL12 and human CXCR4 was determined by RT-PCR. In addition, the peritoneal washings were evaluated for the presence of murine CXCL12 by ELISA. We used primers specific for murine and human CXCL12 (Figure 6A), because under our experimental conditions a band corresponding to human CXCL12 could only be evidenced on human cells but not on murine tissues (Figure 6A). At the same time, primers specific for murine CXCL12 gave a band only when mouse tissues were used (Figure 6A). As shown in Figure 6B, both human and mouse CXCL12 transcripts were undetectable in PBMCs immediately prior to injection; meanwhile, they were both readily evidenced in the cell populations recovered at all the time points considered. On the other hand, the CXCR4 transcript was always consistently detected in all cell populations studied (Figure 6B).

RT-PCR results seemed to indicate that murine CXCL12 is the main isoform present in the early stages of lymphomagenesis. We thus determined whether murine CXCL12 protein was effectively present in the peritoneal cavity and how it varied during the lymphomagenesis process. As shown in Figure 6C, low levels of murine CXCL12 were present in the peritoneal washings prior to PBMC injection; however, during the course of the lymphomagenesis process there was a considerable increase in the protein levels of CXCL12, reaching a peak at the moment of killing.

In view of these data, which suggested the possibility that a CXCL12/CXCR4 autocrine/paracrine loop could be at work in lymphoma development and progression, we wondered whether interfering with the CXCL12/CXCR4 axis could affect lymphoma development in SCID mice. To this end, we chose to use freshly obtained hu/SCID tumor cell suspensions to generate tumors in naive SCID mice. Hu/SCID lymphoma cells were used instead of PBMCs from EBV-positive donors because of the well-known problem of the very high heterogeneity in the generation of lymphomas in SCID mice among different donors,[32,33] which would have complicated the interpretation of the effects of

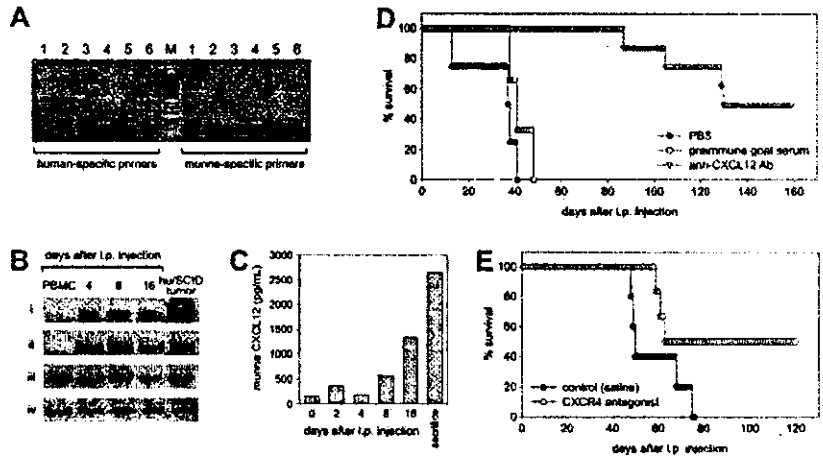

Figure 6. Expression of the CXCL12/CXCR4 axis in vivo following PBMC transfer to SCID mice and effects of CXCL12 and CXCR4 neutralization in vivo. (A) The specificity of our primer pairs for human and murine CXCL12 was evaluated on human and murine samples. A band corresponding to human CXCL12 was detected only on human samples: HUVECs (lane 1), MRC-5 (lane 2), human microvascular endothelial cells (lane 3), and LCLs (lane 5) but not on murine tissues such as the peritoneal membrane (lane 4). Conversely, primers specific for murine CXCL12 gave a band only on murine tissues (lane 4). Lane 6 corresponds to the water control. (B) The expression of CXCL12 and CXCR4 in cells recovered from the peritoneal cavity of SCID mice injected with PBMCs from EBV-positive donors was evaluated by RT-PCR. The cells were analyzed before and after various time intervals following intraperitoneal injection for the expression of human CXCL12 (i), murine CXCL12 (ii), human CXCR4 (iii), and β-actin (iv). The first left lane corresponds to the profile obtained with freshly isolated PBMCs; the last lane corresponds to a hu/SCID tumor sample. (C) Expression of murine CXCL12 as evaluated by ELISA in the peritoneal washings obtained at various time intervals following PBMC transfer in SCID mice. (D-E) Effect of CXCL12 and CXCR4 neutralization on tumor growth. Freshly isolated hu/SCID tumor cell suspensions were injected intraperitoneally into naive SCID mice. (D) Mice were treated with intraperitoneal injections of goat anti-CXCL12 Ab, PBS, or heat-inactivated goat preimmune serum every day for 3 weeks starting from the day after cell transfer. The effect of anti-CXCL12 Ab and treatment on lymphoma development was assessed by effects on survival. Five to 8 mice were included in each experimental group, and the experiment was repeated twice. (E) In another group of animals following PBMC transfer, Alzet pumps releasing the CXCR4 antagonist 4F-benzoyl-TN14003 were implanted subcutaneously and changed every 2 weeks for a total of 2 implants. The effect of treatment with 4F-benzoyl-TN14003 on lymphoma development was assessed by effects on survival and tumor dissemination. Six to 8 mice were included in each experimental group.

neutralization of the CXCR4/CXCL12 axis on lymphoma development. Hu/SCID tumor-injected mice were then treated with intraperitoneal injections of a neutralizing anti-CXCL12 Ab or adequate controls. For CXCR4 neutralization, 4F-benzoyl-TN14003, a recently reported T140 derivative shown to have an increased biostability with respect to TC14012,[18] was administered by subcutaneous injection using Alzet pumps beginning from the day preceding transplantation of hu/SCID lymphoma cells for 4 consecutive weeks. As shown in Figure 6D, in experiments evaluating the effect of CXCL12 neutralization, all control animals succumbed within 50 days after tumor cell transfer; meanwhile, mouse treatment with the neutralizing anti-CXCL12 Ab significantly delayed lymphoma development (Figure 6D; $P < .0002$), with 50% of anti-CXCL12–treated animals being tumor free after 180 days. A similar effect on animal survival was observed when 4F-benzoyl-TN14003 was used (Figure 6E; $P < .05$).

Discussion

In this article we addressed the contribution of the chemokine system to the outgrowth of EBV-positive B-cell lymphomas in SCID mice injected intraperitoneally with PBMCs from EBV-positive donors. We showed that most in vitro–transformed LCLs strongly down-regulated the expression of most chemokine receptors, compared with normal B lymphocytes; meanwhile, most hu/SCID tumors analyzed expressed CXCR3 and CXCR4 at moderately high levels and CCR6, CCR7, and CXCR5 at intermediate/low levels. That in vivo and in vitro immortalization of circulating B cells by EBV is associated with down-regulation of CCR6, CCR7, and CXCR5 expression may be partially linked to the activation state of these cells.[34] Our data concerning LCLs partially confirm those recently reported by other workers,[35] in that we also found a down-regulation of CXCR4 and CXCR5; however, we were not able to document any significant up-regulation of CCR6 surface expression in LCL cells. Notably, only a few LCL samples were considered by these authors[35]; in addition, the modulation of chemokine receptor expression (in comparison with a single peripheral blood B-cell sample examined) was solely based on a semiquantitative RT-PCR analysis,[35] while our conclusions are based on protein expression by cytofluorimetry on a much larger number of samples. On the other hand, this apparent discrepancy might depend on the very high heterogeneity between LCLs, as also encountered in the present study (Figure 1), and the modulation of some chemokine receptors associated with in vitro culture (data not shown). The differential profile of chemokine receptor expression between LCLs and hu/SCID tumor cells, with these latter expressing moderately high CXCR3 and CXCR4 levels, may also partially reflect a different stage of maturation of these 2 cell populations.[28] It is well known that plasma cells express CXCR4 while down-modulating CCR7 and CXCR5,[36] whereas activated B cells down-modulate CCR6 (Brandes et al[34] and data not shown). Thus, the down-regulation of CCR6, CCR7, and CXCR5 seen in hu/SCID tumors may partially reflect their stage of differentiation and their activation state.

Recently, it has been described that EBV latent genes can also modify chemokine receptor expression.[35] Hu/SCID tumors in general exibit low levels of latent EBV transcripts such as Epstein-Barr nuclear antigen-1 (EBNA-1), EBNA-2, and latent membrane protein-1 (LMP-1) with respect to LCLs.[5] Thus, differential expression of EBV latent genes between LCLs and hu/SCID tumors may also help explain the differences in the chemokine receptor profile between LCLs and hu/SCID tumors. In this regard, as outlined previously and reported by others,[5,28] hu/SCID tumors are composed of 2 phenotypically distinct B-cell subsets: $CD23^{low}CD38^{hi}$ and $CD23^{int}CD38^{int}$; meanwhile, LCLs have been

reported to be homogenously $CD23^{hi}CD38^{int/low}$.[5,28] The $CD23^{low}CD38^{hi}$ cell population present within hu/SCID tumors expresses lytic cycle EBV transcripts, while the $CD23^{int}CD38^{int}$ population only expresses the latent cycle transcripts EBNA-1, EBNA-2, and LMP-1.[5] We demonstrated that surface CXCR4 is predominantly expressed by the $CD23^{low}$ tumor cell subset, previously shown to have a low proliferative index and high-level Ig secretion, typical of plasma cells.[5] Thus, it is conceivable that differential expression of EBV genes could translate into modulation of chemokine receptor expression, with CXCR4 up-regulation by lytic gene products.

Given these premises, we concentrated our attention on the CXCR4 ligand, CXCL12, to evaluate whether a putative autocrine loop could be at work in the lymphomagenesis process of this experimental model. We showed for the first time that EBV-transformed B cells, both LCLs and hu/SCID tumors, are able to express CXCL12, in contrast to resting and in vitro–activated B lymphocytes. Interestingly, CXCL12 was shown to be produced predominantly by the $CD23^{int}$ tumor cell subset, which expresses low levels of surface CXCR4 (sCXCR4) but high levels of internal CXCR4. It has been previously shown that the transfer of a tumor cell line (generated after in vitro growth of hu/SCID lymphomas) expressing CD23 at intermediate levels to SCID mice entails a substantial shift to low CD23 expression. Because the former expresses low levels of sCXCR4, while the latter expresses good levels of sCXCR4, it could be inferred that the $CD23^{int}CD38^{int}sCXCR4^{low}$ (lymphoblastoid-like) subset shifts phenotype to $CD23^{low}CD38^{hi}sCXCR4^{int}$ (plasmacytoid-like) after transfer and growth in SCID mice with gain of CXCL12 responsiveness and that the plasmacytoid cells originate from the lymphoblastoid cells.[28] We thus expand the current knowledge regarding this experimental model, proposing that the differentiation of plasmacytoid cells from lymphoblastoid cells involves gain of CXCR4 surface expression (and responsiveness) and reduced production of CXCL12 and that the CXCL12/CXCR4 axis may be important in the homeostasis of the 2 tumor subsets that are found within lymphomas. Furthermore, in vitro treatment of hu/SCID lymphoma cells with neutralizing ant-CXCL12 Abs or TC14012 decreased cell survival and proliferation, implying autocrine regulation of hu/SCID lymphoma cell biology by endogenous CXCL12. However, the fact that blocking CXCR4 or CXCL12 reduced but did not completely inhibit the proliferation and survival of hu/SCID lymphoma cells suggests that factors and pathways other than CXCR4/CXCL12 interactions are involved in the regulation of these processes. Further work is warranted to clarify this issue.

Along with the demonstration that CXCL12 expression by B lymphocytes could be related to EBV transformation, one major finding of this work is the demonstration that interfering with the CXCL12/CXCR4 axis may affect EBV-transformed cell behavior, both in vitro and in vivo. Indeed, we found that the lymphomagenesis process was associated with a dramatic increase in the levels of murine CXCL12 present within the peritoneal cavity, suggesting a role for this chemokine in lymphoma growth and progression. Notably, with the ELISA kit that was used, human CXCL12 (SDF-1α) exhibits 26% to 42% cross-reactivity at all concentrations, so the contribution of human CXCL12 to tumor growth cannot be completely excluded. In vivo neutralization of the CXCL12/CXCR4 axis by a neutralizing anti-CXCL12 Ab or CXCR4 antagonist had a dramatic effect on lymphoma development, even though the anti-CXCL12 antiserum seemed more effective. The CXCR4 antagonist used in vivo was 4F-benzoyl-TN14003 instead of TC14012, because the latter has been shown to be relatively unstable in rat liver homogenates while 4F-benzoyl-TN14003 is relatively stable in vivo.[18] The minor efficacy of 4F-benzoyl-TN14003 compared with the neutralizing anti-CXCL12 Abs may reflect the greater difficulties of the former with respect to administration modality, schedule, and in vivo stability or half-life. Indeed, only high doses of this antagonist inhibited proliferation and cell survival in vitro.

The neutralization of CXCR4 through the use of an anti-CXCR4 Ab has been shown to be able to prevent tumor growth in nonobese diabetic (NOD)/SCID mice injected intraperitoneally with the Namalwa cell line[13]; however, compared with PBMC-injected SCID mice, this experimental model may be more distant from the human lymphomagenesis setting. In addition, the use of an anti-CXCR4 Ab as a tumor-preventing tool may give a less mechanistic insight into the relevance of the CXCL12/CXCR4 axis in the lymphomagenesis process; in fact, it could be argued that the effect on lymphoma growth could be due to tumor cell elimination by the mouse reticuloendothelial system. We chose to prevent this possible criticism through the use of an Ab directed against CXCL12 and a CXCR4-specific antagonist. In any case, these findings strongly suggest that the CXCR4/CXCL12 axis could play a significant role in favoring the outgrowth and dissemination of EBV-transformed cells in PBMC-injected SCID mice. Because CXCR4 expression has been proven in the human tumor counterpart of this experimental model,[13,14] the CXCL12/CXCR4 axis could indeed become an attractive target for therapy in lymphoma-bearing patients, possibly through the use of small molecular antagonists of CXCR4.

Acknowledgments

We are grateful to Dr J. Gordon (Birmingham, United Kingdom) for providing us with the CD-32L cells. We are particularly indebted to Prof R. M. Strieter (UCLA) for providing the goat anti-CXCL12 serum. We also thank Dr A. Janowska-Wieczorek (Edmonton, AB, Canada) for kind advice on the chemoinvasion assay and Dr K. Balabanian (INSERM U131, Institut Paris-Sud sur les Cytokines, Clamart, France) for help with actin polymerization experiments. Also, the great expertise of Dr A. Rosato in animal procedures is acknowledged. The invaluable help of P. Gallo in artwork preparation is gratefully acknowledged.

References

1. Rickinson AB, Kieff E. Epstein-Barr virus. In: Fields BN, Knipe DM, Howley PM, eds. Fields Virology. Philadelphia, PA: Lippincott-Raven; 2001:2511-2627.
2. Bosma GC, Custer RP, Bosma MJ. A severe combined immunodeficiency mutation in the mouse. Nature. 1983;301:527-530.
3. Custer RP, Bosma GC, Bosma MJ. Severe combined immunodeficiency (SCID) in the mouse: pathology, reconstitution, neoplasms. Am J Pathol. 1985;120:464-477.
4. Mosier DE, Gulizia RJ, Baird SM, Wilson DB. Transfer of a functional human immune system to mice with severe combined immunodeficiency. Nature. 1988;335:256-259.
5. Rochford R, Mosier DE. Differential Epstein-Barr virus gene expression in B-cell subsets recovered from lymphomas in SCID mice after transplantation of human peripheral blood lymphocytes. J Virol. 1995;69:150-155.
6. Amadori A, Veronesi A, Coppola V, Indraccolo S, Mion M, Chieco-Bianchi L. The hu-PBL-SCID mouse in human lymphocyte function and lymphomagenesis studies: achievements and caveats. Semin Immunol. 1996;8:249-254.
7. Veronese ML, Veronesi A, D'Andrea E, et al. Lymphoproliferative disease in human peripheral blood mononuclear cell-injected SCID mice, I: T

lymphocyte requirement for B cell tumor generation. J Exp Med. 1992;176:1763-1767.

8. Johannessen I, Asghar M, Crawford DH. Essential role for T cells in human B-cell lymphoproliferative disease development in severe combined immunodeficient mice. Br J Haematol. 2000;109: 600-610.
9. Piovan E, Bonaldi L, Indraccolo S, et al. Tumor outgrowth in peripheral blood mononuclear cell-injected SCID mice is not associated with early Epstein-Barr virus reactivation. Leukemia. 2003; 17:1643-1649.
10. Muller A, Homey B, Soto H, et al. Involvement of chemokine receptors in breast cancer metastasis. Nature. 2001;410:50-56.
11. Foussat A, Balabanian K, Amara A, et al. Production of stromal cell-derived factor 1 by mesothelial cells and effects of this chemokine on peritoneal B lymphocytes. Eur J Immunol. 2001;31:350-359.
12. Vicente-Manzanares M, Montoya MC, Mellado M, et al. The chemokine SDF-1alpha triggers a chemotactic response and induces cell polarization in human B lymphocytes. Eur J Immunol. 1998;28: 2197-2207.
13. Bertolini F, Dell'Agnola C, Mancuso P, et al. CXCR4 neutralization, a novel therapeutic approach for non-Hodgkin's lymphoma. Cancer Res. 2002;62:3106-3112.
14. Arai J, Yasukawa M, Yakushijin Y, Miyazaki T, Fujita S. Stromal cells in lymph nodes attract B-lymphoma cells via production of stromal cell-derived factor-1. Eur J Haematol. 2000;64:323-332.
15. Amadori A, Zamarchi R, Ciminale V, et al. HIV-1-specific B cell activation: a major constituent of spontaneous B cell activation during HIV-1 infection. J Immunol. 1989;143:2146-2152.
16. Wheeler K, Gordon J. Co-ligation of surface IgM and CD40 on naive B lymphocytes generates a blast population with an ambiguous extrafollicular/germinal centre cell phenotype. Int Immunol. 1996;8:815-828.
17. Phillips RJ, Burdick MD, Lutz M, Belperio JA, Keane MP, Strieter RM. The stromal derived factor-1/CXCL12-CXC chemokine receptor 4 biological axis in non-small cell lung cancer metastases. Am J Respir Crit Care Med. 2003;167:1676-1686.
18. Tamamura H, Hori A, Kanzaki N, et al. T140 analogs as CXCR4 antagonists identified as anti-metastatic agents in the treatment of breast cancer. FEBS Lett. 2003;550:79-83.
19. Lataillade JJ, Clay D, Bourin P, et al. Stromal cell-derived factor 1 regulates primitive hematopoiesis by suppressing apoptosis and by promoting G(0)/G(1) transition in CD34(+) cells: evidence for an autocrine/paracrine mechanism. Blood. 2002;99:1117-1129.
20. Ghia P, Transidico P, Veiga JP, et al. Chemoattractants MDC and TARC are secreted by malignant B-cell precursors following CD40 ligation and support the migration of leukemia-specific T cells. Blood. 2001;98:533-540.
21. Indraccolo S, Gola E, Rosato A, et al. Differential effects of angiostatin, endostatin and interferon-alpha(1) gene transfer on in vivo growth of human breast cancer cells. Gene Ther. 2002;9:867-878.
22. De Clerck LS, Bridts CH, Mertens AM, Moens MM, Stevens WJ. Use of fluorescent dyes in the determination of adherence of human leucocytes to endothelial cells and the effect of fluorochromes on cellular function. J Immunol Methods. 1994; 172:115-124.
23. Kijowski J, Baj-Krzyworzeka M, Majka M, et al. The SDF-1-CXCR4 axis stimulates VEGF secretion and activates integrins but does not affect proliferation and survival in lymphohematopoietic cells. Stem Cells. 2001;19:453-466.
24. Tamamura H. Development of selective antagonists against an HIV second receptor [in Japanese]. Yakugaku Zasshi. 2001;121:781-792.
25. Trentin L, Cabrelle A, Facco M, et al. Homeostatic chemokines drive migration of malignant B cells in patients with non-Hodgkin lymphomas. Blood. 2004;104:502-508.
26. Janiak M, Hashmi HR, Janowska-Wieczorek A. Use of the Matrigel-based assay to measure the invasiveness of leukemic cells. Exp Hematol. 1994;22:559-565.
27. Indraccolo S, Minuzzo S, Zamarchi R, Calderazzo F, Piovan E, Amadori A. Alternatively spliced forms of Igalpha and Igbeta prevent B cell receptor expression on the cell surface. Eur J Immunol. 2002;32:1530-1540.
28. Rochford R, Hobbs MV, Garnier JL, Cooper NR, Cannon MJ. Plasmacytoid differentiation of Epstein-Barr virus-transformed B cells in vivo is associated with reduced expression of viral latent genes. Proc Natl Acad Sci U S A. 1993;90:352-356.
29. Yokoi T, Miyawaki T, Yachie A, Kato K, Kasahara Y, Taniguchi N. Epstein-Barr virus-immortalized B cells produce IL-6 as an autocrine growth factor. Immunology. 1990;70:100-105.
30. Tosato G, Jones K, Breinig MK, McWilliams HP, McKnight JL. Interleukin-6 production in post-transplant lymphoproliferative disease. J Clin Invest. 1993;91:2806-2814.
31. Peled A, Grabovsky V, Habler L, et al. The chemokine SDF-1 stimulates integrin-mediated arrest of CD34(+) cells on vascular endothelium under shear flow. J Clin Invest. 1999;104:1199-1211.
32. Picchio GR, Kobayashi R, Kirven M, Baird SM, Kipps TJ, Mosier DE. Heterogeneity among Epstein-Barr virus-seropositive donors in the generation of immunoblastic B-cell lymphomas in SCID mice receiving human peripheral blood leukocyte grafts. Cancer Res. 1992;52:2468-2477.
33. Coppola V, Veronesi A, Indraccolo S, et al. Lymphoproliferative disease in human peripheral blood mononuclear cell-injected SCID mice, IV: Differential activation of human Th1 and Th2 lymphocytes and influence of the atopic status on lymphoma development. J Immunol. 1998;160: 2514-2522.
34. Brandes M, Legler DF, Spoerri B, Schaerli P, Moser B. Activation-dependent modulation of B lymphocyte migration to chemokines. Int Immunol. 2000;12:1285-1292.
35. Nakayama T, Fujisawa R, Izawa D, Hieshima K, Takada K, Yoshie O. Human B cells immortalized with Epstein-Barr virus upregulate CCR6 and CCR10 and downregulate CXCR4 and CXCR5. J Virol. 2002;76:3072-3077.
36. Hargreaves DC, Hyman PL, Lu TT, et al. A coordinated change in chemokine responsiveness guides plasma cell movements. J Exp Med. 2001; 194:45-56.

Identification of a CXCR4 antagonist, a T140 analog, as an anti-rheumatoid arthritis agent

Hirokazu Tamamura[a,*], Miho Fujisawa[b], Kenichi Hiramatsu[a], Makiko Mizumoto[a], Hideki Nakashima[c], Naoki Yamamoto[d], Akira Otaka[a], Nobutaka Fujii[a,*]

[a]*Graduate School of Pharmaceutical Sciences, Kyoto University, Sakyo-ku, Kyoto 606-8501, Japan*
[b]*Takeda Chemical Industries, Ltd., Pharmaceutical Research Division, Yodogawa-ku, Osaka 532-8686, Japan*
[c]*School of Medicine, St. Marianna University, Miyamae-ku, Kawasaki 216-8511, Japan*
[d]*School of Medicine, Tokyo Medical and Dental University, Bunkyo-ku, Tokyo 113-8519, Japan*

Received 24 March 2004; revised 7 May 2004; accepted 11 May 2004

Available online 7 June 2004

Edited by Beat Imhof

Abstract Several recent papers support the involvement of an interaction between stromal cell-derived factor-1 (SDF-1/CXCL12) and its receptor, chemokine receptor CXCR4, in memory T cell migration in the inflamed rheumatoid arthritis (RA) synovium. Analogs of the 14-mer peptide T140 were previously found to be specific CXCR4 antagonists that were characterized as not only HIV-entry inhibitors but also anti-cancer-metastatic agents. In this study, a T140 analog, 4F-benzoyl-TN14003, was proven to inhibit CXCL12-mediated migration of human Jurkat cells and mouse splenocyte in a dose-dependent manner in vitro (IC_{50} = 0.65 and 0.54 nM, respectively). Furthermore, slow release administration by subcutaneous injection (s.c.) of 4F-benzoyl-TN14003 using an Alzet osmotic pump significantly suppressed the delayed-type hypersensitivity response induced by sheep red blood cells in mice, and significantly ameliorated clinical severity in collagen-induced arthritis in mice. As such, T140 analogs might be attractive lead compounds for chemotherapy of RA.

Keywords: CXCR4 antagonist; Rheumatoid arthritis; T140; Collagen-induced arthritis; Delayed-type hypersensitivity

1. Introduction

Inflammatory cytokines, such as IL-1, IL-6, IFN-γ and tumor necrosis factor (TNF)-α, and activation markers play a central role in the chronic rheumatoid arthritis (RA) synovium [1]. Development of biological drugs targeting these cytokines, such as humanized monoclonal antibodies, has produced promising results in clinical therapy of RA patients. However, this therapy has not yet reached a stage of perfection, and development of other drugs with novel action mechanisms that are independent of the above cytokine's functions, is required for the improvement of RA chemotherapy. Intrinsically, RA is caused by the $CD4^+$ memory T cell accumulation in the inflamed synovium. Nanki et al. [2] reported that the memory T cells highly express a chemokine receptor CXCR4, and that the concentration of stromal cell-derived factor-1 (SDF-1/CXCL12), an endogenous ligand of CXCR4, is extremely high in the synovium of RA patients compared to controls. They also found that CXCL12 stimulates migration of the memory T cells and inhibits T cell apoptosis, suggesting that the CXCL12–CXCR4 interaction plays an important role in T cell accumulation in the RA synovium. Since chemokine CXCL12 [3–6] is independent of the inflammatory cytokines such as TNF-α, in terms of its expression and action, development of substances that inhibit the CXCL12–CXCR4 interaction might be promising as drugs. We have developed several CXCR4 antagonists, T22 (an 18-mer peptide) [7], T140 (a 14-mer) [8] and FC131 (a cyclic pentapeptide) [9]. These peptides have inhibitory activity against entry of T-cell line-tropic (X4-) HIV-1 into target cells [7,10,11] as well as against cancer metastasis and progression in breast cancer [12], pancreatic cancer [13,14], melanoma [15], acute lymphoblastic leukemia [16], small cell lung cancer [17], etc. In this study, we investigated whether a bio-stable T140 analog, 4F-benzoyl-TN14003 [18], shows anti-RA activity in the following experiments: inhibition assays of Jurkat cell/splenocyte migration mediated by CXCL12 in vitro, the delayed-type hypersensitivity (DTH) response induced by sheep red blood cells (SRBC) in vivo and collagen-induced arthritis (CIA) in vivo.

2. Material and methods

2.1. Material

4F-benzoyl-TN14003 [4-fluorobenzoyl–Arg–Arg–Nal–Cys–Tyr–Cit–Lys–D–Lys–Pro–Tyr–Arg–Cit–Cys–Arg–NH_2, a disulfide bond between Cys^4–Cys^{13}, Nal = L-3-(2-naphthyl)alanine, Cit = L-citrulline] was previously synthesized [18,19].

2.2. Migration assay of human Jurkat cells

Human Jurkat cells were obtained from the American Type Culture Collection (Manassas, VA, USA), and cultured in RPMI-1640 medium (BioWhittaker, Walkersville, MD, USA) supplemented with 10% fetal calf serum (BioWhittaker).

Jurkat cells (2.5×10^6 cells/ml) were pre-incubated with various concentrations of 4F-benzoyl-TN14003 at 37 °C for 30 min. Then 200 μl of this suspension was placed into Transwell (Corning-Costar, Cambridge, MA, USA) culture inserts within 24-well culture plates containing 600 μl of assay medium (RPMI-1640/0.5% BSA/50 mmol/l HEPES) with 10 ng/ml human CXCL12 (Genzyme Techne, Minneapolis, MN, USA). The plates were incubated at 37 °C for 4 h in a humidified 5% CO_2 incubator. After the incubation, the culture inserts

* Corresponding authors. Fax: +81-75-753-4570.
E-mail addresses: tamamura@pharm.kyoto-u.ac.jp (H. Tamamura), nfujii@pharm.kyoto-u.ac.jp (N. Fujii).

0014-5793/$22.00
doi:10.1016/j.febslet.2004.05.056

were removed and migrated cells from the inserts into the wells were counted using a Coulter counter. Percent migration was based on the total initial input per well.

2.3. Mouse splenocyte preparation and migration assay

Spleens were isolated from BALB/c mice (male, Charles River, Yokohama, Japan), and single-cell suspensions prepared from spleens were incubated in RBC lysing buffer (Immuno-Biological Laboratories, Fujioka, Japan), washed twice with PBS and then resuspended in assay medium.

Chemotaxis was measured in a 2.5-h Transwell migration assay as described above. Recombinant mouse CXCL12 (100 ng/ml, PeproTech, London, UK) was added to the wells in chemotaxis medium, and 1×10^7 cells were added to the Transwell inserts. Migrated cells were counted with a Coulter counter.

2.4. Inhibition assay of the mouse DTH response

SRBC were washed twice with saline, and then resuspended in saline. BALB/c mice (male 6 weeks, Charles River) were sensitized with a subcutaneous injection of 5×10^7 SRBC in 50 μl of saline into the left hind footpad. Five days later, mice were challenged by subcutaneously injecting 1×10^8 SRBC in 50 μl of saline into the right hind footpad. The thickness of the right hind paw was measured with a micrometer (Mitutoyo, CD-15B, Kawasaki, Japan) before treatment and 24 h after challenge. The DTH reaction was expressed as the swelling of the right footpad.

2.5. Induction and evaluation of CIA

Bovine type II collagen (CII, Collagen Research Center, Tokyo, Japan) was dissolved in 0.05 mol/l acetic acid to a concentration of 2 mg/ml, and the emulsion was prepared with an equal volume of Freund's complete adjuvant (Difco, Detroit, MI, USA).

Six week-old male DBA/1J mice (Charles River) were injected intradermally at the base of the tail with a volume of 50 μl of the above emulsion. Twenty-one days after immunization, mice were given booster shots with the CII emulsion in the same manner. Following this injection, mice were evaluated for the incidence and the severity of arthritis, body weight and the thickness of the hind ankles, twice a week. At the end of the experimental period (2 weeks after the second injection), sera were obtained and the weights of the 4 limbs were measured.

The clinical severity of the arthritis was graded on a scale of 0–3 for each paw as follows: 0, normal; 1, swelling of one digit or mild swelling of the paw; 2, swelling of multiple digits or moderate swelling of the entire paw; 3, severe swelling of the entire paw. Each mouse could achieve a maximum score of 12.

2.6. Measurement of serum anti-bovine CII antibody

Levels of serum anti-bovine CII IgG2a antibody were measured using an ELISA assay. 96-well immunoplates were coated with bovine CII (10 μg/ml in PBS) and incubated at 4 °C overnight. Non-specific binding was blocked with PBS containing 10% FCS for 2 h. Mouse serum samples diluted with 10% FCS in PBS (1:1000) were added to the wells and incubated at room temperature for 2 h. Horseradish peroxidase-conjugated rat anti-mouse IgG2a antibody (1:1000 diluted, Zymed Laboratories, South San Francisco, CA, USA) was added and incubated for 1 h. 3,3′,5,5′-Tetramethylbenzidine (TMB) substrate solution (DAKO A/S, Glostrup, Denmark) was added and allowed to react for 30 min. The reaction was stopped by the addition of an equal volume of 1 mol/l H_2SO_4, and the optical density at 450 nm was measured using a microplate reader (Labsystems MultiscanMS, Helsinki, Finland). For this ELISA, the wells were washed with PBS containing 0.1% Tween 20 before each step.

2.7. Drug administration

4F-benzoyl-TN14003 was dissolved in PBS, and subcutaneously administered using Alzet osmotic pumps (DURECT Corp., Cupertino, CA, USA), which were implanted dorsalaterally under the skin at the day before immunization (DTH) or the booster (CIA). In the experiment of DTH and CIA, #1007D pumps (delivering 4.8, 24 and 120 μg/day of 4F-benzoyl-TN14003 for 7 days) and # 2002 ones (delivering 120 μg of 4F-benzoyl-TN14003 daily for 14 days) were used, respectively. Indomethacin (1 mg/kg, Sigma Chemicals Co., St. Louis, MO, USA), methotrexate (3 mg/kg, Wako Pure Chemical Industries, Ltd, Osaka, Japan) and FK-506 (10 mg/kg, purified in Takeda Chemical Industries, Ltd, Osaka, Japan) were orally administered once daily for 2 weeks from the day of booster. These drugs were suspended in a 0.5% methylcellulose solution.

2.8. Statistical analysis

The values were represented as the means ± S.E. Statistical differences were determined using an analysis of variance (ANOVA, SAS software, version 6.1, SAS Institute, Cary, NC, USA). Results of DTH were assessed with the one-tailed Williams' test. A value of $P \leqslant 0.025$ was considered statistically significant. In the experiment involving CIA, unpaired or paired *t*-test were applied when only two values sets were compared. When data involved three or more groups, statistical analysis was performed using Dunnett's test. Clinical scores for each group were compared using the non-parametric Steel test or the Wilcoxon rank-sum test. The level of significance was defined as $P \leqslant 0.05$ and $P \leqslant 0.01$.

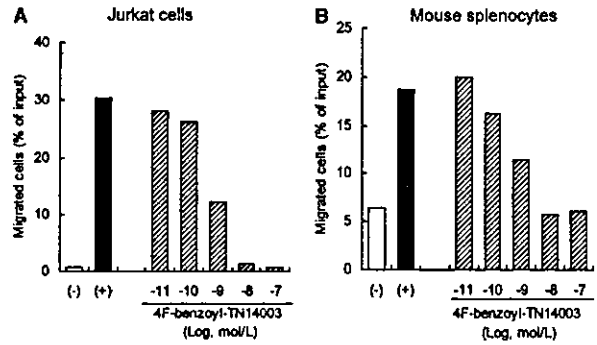

Fig. 1. Effects of 4F-benzoyl-TN14003 on CXCL12-induced migration of human Jurkat cells (A) and mouse splenocytes (B). Both cells were treated by CXCL12 (human CXCL12 10 ng/ml for Jurkat cells, mouse CXCL12 100 ng/ml for splenocytes) and various concentrations of 4F-benzoyl-TN14003. Control migrating cells in the absence and presence of CXCL12 are shown as (−) and (+), respectively. Data are expressed as means ($n = 2$).

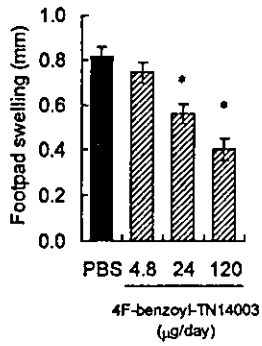

Fig. 2. Inhibition of the mouse DTH response by 4F-benzoyl-TN14003. The gain of thickness of right footpad by swelling 24 h after challenge was measured by a micrometer. PBS (control models) or 4F-benzoyl-TN14003 (4.8, 24 or 120 μg/day) was administered by s.c. injection using an Alzet pump from the day before immunization. Data are expressed as means ± S.E. ($n = 7$). * $P \leqslant 0.025$ (Williams' test).

3. Results

3.1. Inhibition of migration of human Jurkat cells and mouse splenocytes

Both human Jurkat cells and mouse splenocytes express CXCR4 on their surfaces [12,20]. CXCL12 (10 ng/ml = 1.1 nM for Jurkat cells, 100 ng/ml = 11 nM for splenocytes) dramatically enhanced the migration of Jurkat cells and splenocytes, as compared to control (absence of CXCL12, Fig. 1). 4F-benzoyl-TN14003 inhibited CXCL12-induced migration of these cells in a dose-dependent manner. At a concentration of 10 nM, 4F-benzoyl-TN14003 showed approximately 100% inhibition of cell migration induced by CXCL12 (1.1 nM for Jurkat cells, 11 nM for splenocytes). The IC_{50} values were determined to be 0.65 nM and 0.54 nM, respectively.

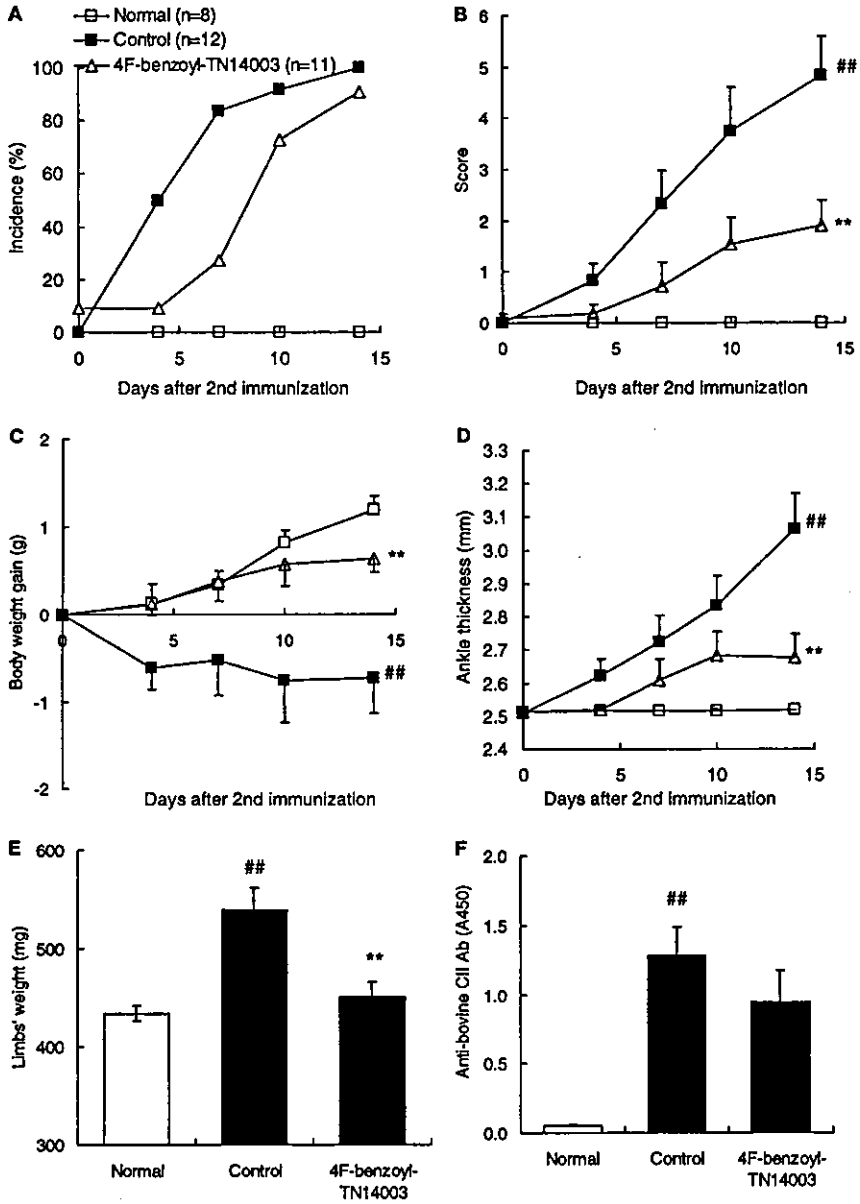

Fig. 3. Suppression of CIA in mice by 4F-benzoyl-TN14003. The incidence (A) and the score expressing the clinical severity (B) of arthritis were evaluated, and body weight (C) and the thickness of the hind ankles (D) were measured after the second immunization twice a week. The weights of 4 limbs were measured 2 weeks after the second immunization (E). Levels of anti-bovine CII IgG2a antibody in serum, which was obtained 2 weeks after the second immunization, were measured by ELISA (F). PBS (control models, $n = 12$) or 4F-benzoyl-TN14003 (120 μg/day, $n = 11$) was administered by s.c. injection using an Alzet pump from the day before the second immunization. In normal models ($n = 8$), mice were not immunized. Data are expressed as means ± S.E. $^{\#\#}P \leqslant 0.01$ (t-test): comparison with normal models, $^{**}P \leqslant 0.01$ (t-test): comparison with control models (Scores were compared by non-parametric Steel test).

3.2. Reduction of the DTH reaction in mice by subcutaneous administration of 4F-benzoyl-TN14003 using Alzet osmotic pumps

The SRBC-induced DTH reaction in mice was adopted as an in vivo experimental model of the cellular immune response for evaluation of 4F-benzoyl-TN14003 activity. The DTH reaction was estimated as the gain of right footpad thickness from swelling, 24 h after challenge. Seven mice were administered PBS as control models and showed significant footpad swelling (Fig. 2). Twenty one mice were administered 4F-benzoyl-TN14003 by s.c. injection using Alzet pumps (delivering 4.8, 24 and 120 μg/day, each for 7 mice) beginning from the day before immunization. Treated mice showed a dose-dependent suppression of swelling, as compared to control mice. The 24 and 120 μg daily injections showed inhibitory percentages of 31% and 51%, respectively. 4F-benzoyl-TN14003 significantly reduced the DTH reaction in mice.

3.3. Suppression of CIA in mice by subcutaneous administration of 4F-benzoyl-TN14003 using Alzet osmotic pumps

In the next phase, CIA was adopted to provide a second in vivo mouse model of this pathogenesis. During the 2 weeks after the CII emulsion booster, the following data were collected: the arthritis incidence, the scores expressing the severity, the body weight and thickness of the hind ankles were observed twice a week; the 4 limbs' weights and the serum anti-bovine CII antibodies were measured on the 14th day. Eleven mice were administered 4F-benzoyl-TN14003 by s.c. injection using Alzet pumps (delivering 120 μg/day), beginning from the day before the booster. Twelve mice were administered PBS as control models. Eight mice were not immunized as normal models. After observation for 14 days, 4F-benzoyl-TN14003-treated mice showed significant suppression of several symptoms of arthritis (score increase, body weight loss, ankle swelling and limbs' weight gain) as compared to the control mice that developed arthritis (Figs. 3 and 4). 4F-benzoyl-TN14003-treated mice also showed an apparent suppression of the extreme increase in levels of serum anti-bovine CII IgG2a antibody observed for the control group (Fig. 3F).

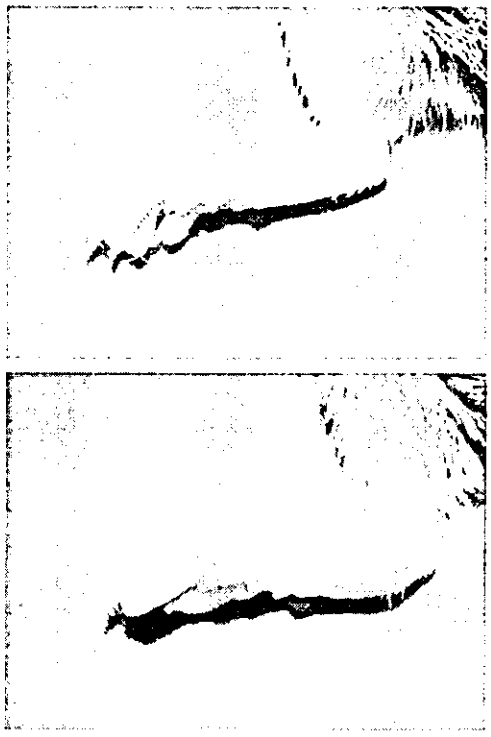

Fig. 4. Reduction of ankle swelling in mouse CIA by 4F-benzoyl-TN14003. Representative hind ankles of mice 2 weeks after the second immunization are shown. *Upper*, 4F-benzoyl-TN14003 was administered by s.c. injection using an Alzet pump from the day before the second immunization; *Lower*, PBS was administered as control models.

In a further comparative study, indomethacin [21] (1 mg/kg), methotrexate [22] (3 mg/kg) and FK-506 [23] (10 mg/kg), which are clinically used for treatment of RA patients or are known as anti-RA agents, were orally administered once daily for 2 weeks from the day of the booster (Fig. 5). These treated mice showed significant suppression of ankle swelling and limb weight gain, and an apparent suppression of marked increases in arthritis scores and anti-bovine CII antibody levels, remarkably similar to the results with 4F-benzoyl-TN14003. Therefore, 4F-benzoyl-TN14003 can be seen to possess inhibitory activity against RA symptoms, comparable to these known drugs.

4. Discussion

Chemokines constitute a chemotactic cytokine family that attract and induce migration of leukocytes, playing a fundamental role in the physiology of inflammation. CXCL12 is a chemokine that recognizes CXCR4. CXCR4 also has significant involvement in several pathological conditions, including AIDS [24], cancer [12–17,25] and RA [2]. The pathological importance of CXCR4 derives from its initial identification as the second receptor involved in the X4-HIV-1 entry into T cells [24]. According to recent reports, CXCL12 induces migration of several types of cancer cells via CXCR4 on their cell surfaces, causing cancer metastasis and progression [12–17,25]. Furthermore, the CXCL12/CXCR4 axis is thought to play an important role in the rheumatoid T cell accumulation in RA, as described in Section 1 [2]. Thus, CXCR4 represents an important therapeutic target for these diseases. We have previously developed several CXCR4 antagonists, T22, T140, 4F-benzoyl-TN14003 and FC131, which have strong anti-HIV-1 and anti-cancer metastatic activities, as described in Section 1 [7–17]. De Clercq's group reported another CXCR4 antagonist, AMD3100, which also has strong anti-HIV-1 activity [26]. Recently, he and his colleagues have found that AMD3100 inhibits autoimmune joint inflammation in IFN-γ receptor-deficient mice, and that AMD3100 interferes with cellular DTH reaction, but not with the humoral immune response to CII in CIA, as assessed by measuring anti-CII antibody levels [20]. In this study, we investigated whether 4F-benzoyl-TN14003 shows anti-RA activity by assessing its effects on humoral and cellular immunity.

We previously reported that 4F-benzoyl-TN14003 has strong binding capacity to CXCR4, as shown by inhibition of [^{125}I]-CXCL12 binding to CXCR4-expressing human Jurkat cells (IC_{50} = 0.99 nM) [12]. In this study, 4F-benzoyl-TN14003 was clearly shown to inhibit CXCL12-induced migration of Jurkat cells in a dose-dependent manner at subnanomolar levels, and also to inhibit mouse splenocyte migration induced by CXCL12. These results suggest that the activity of this com-

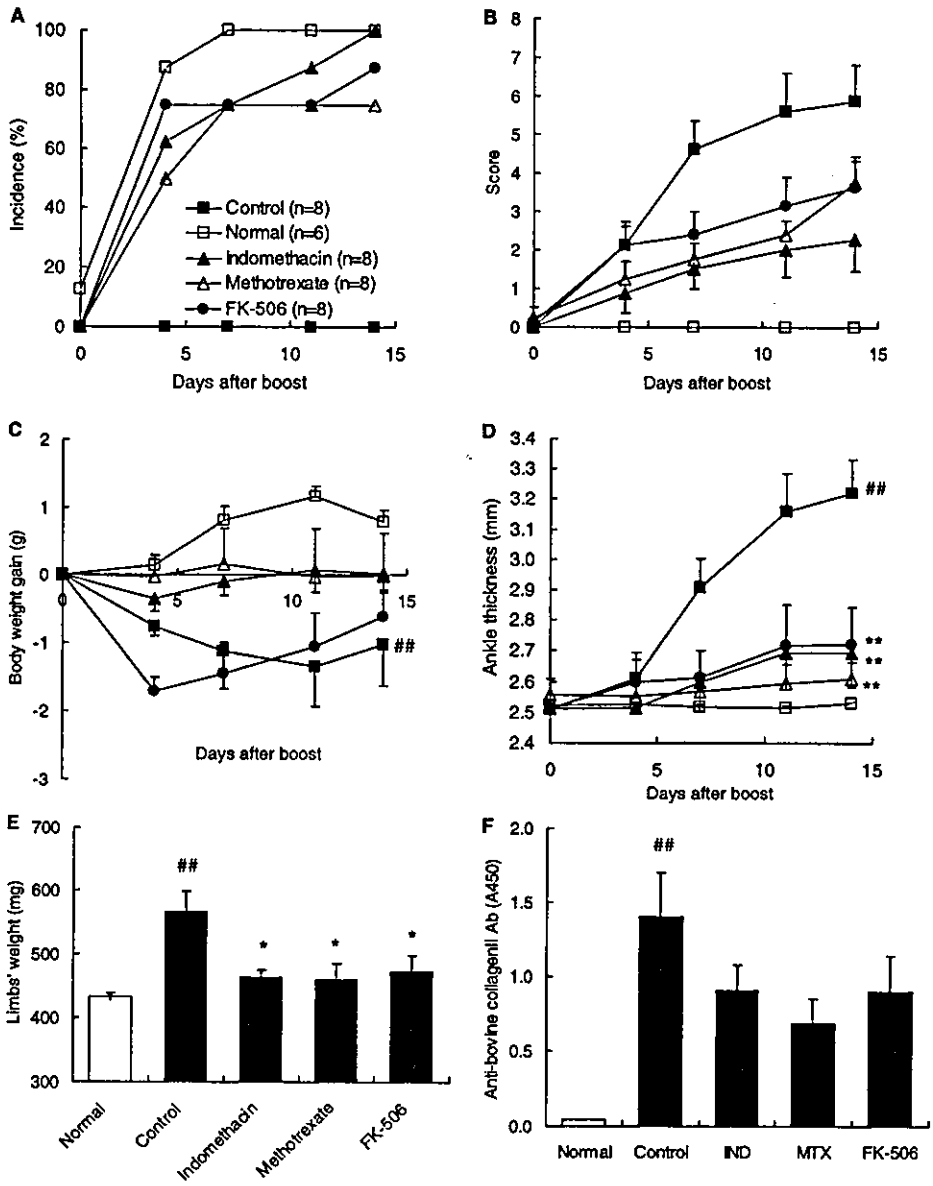

Fig. 5. Suppression of CIA in mice by known drugs. Efficacies of drugs were evaluated in the same way as in the experiments of Fig. 3 (A–F). PBS (control models, $n = 8$), indomethacin (1 mg/kg, $n = 8$), methotrexate (3 mg/kg, $n = 8$) or FK-506 (10 mg/kg, $n = 8$) was orally administered from the day of the second immunization once daily for 2 weeks. In normal models ($n = 6$), mice were not immunized. Data are expressed as means ± S.E. $^{\#\#}P \leqslant 0.01$ (t-test): comparison with normal models, $^{*}P \leqslant 0.05$ and $^{**}P \leqslant 0.01$ (Dunnett's test): comparison with control models.

pound is species independent, possibly due to the close homology of human and mouse CXCR4 [27]. Evaluation of the inhibitory activity of 4F-benzoyl-TN14003 against CXCL12-induced migration of CXCR4-expressing T cells suggests that 4F-benzoyl-TN14003 inhibits CXCL12-stimulated migration of memory T cells, thereby suppressing accumulation of T cells caused by inhibition of their apoptosis in the inflamed synovium of RA patients. Therefore, we investigated the inhibitory effects of 4F-benzoyl-TN14003 against RA using two mouse experimental models: the DTH response and CIA.

To evaluate the effect of 4F-benzoyl-TN14003 on cellular immunity, the DTH reactivity induced by SRBC was examined in mice. Subcutaneous administration of 4F-benzoyl-TN14003 using Alzet osmotic pumps significantly suppressed the footpad swelling. This indicates that 4F-benzoyl-TN14003 interferes with cellular immunity such as DTH, suggesting that CXCR4 might play an important role in cellular immunity.

Next, the activity of 4F-benzoyl-TN14003 was assessed in the CIA experiment, an RA animal model. The levels of several CIA symptoms were significantly lower in 4F-benzoyl-TN14003-treated mice than those in PBS-treated mice (arthritic control mice). Serum levels of the anti-CII IgG2a anti-body were also apparently lower in 4F-benzoyl-TN14003-treated mice. 4F-benzoyl-TN14003 therefore interferes with the humoral immune

response to CII, in contrast to AMD3100 [20]. The differences in the actions of AMD3100 and 4F-benzoyl-TN14003 in humoral CIA immunity might be explained by a difference in the binding sites of these CXCR4 antagonists [28] or by differences in the CIA models that were used.

In conclusion, the present results suggest that a bio-stable T140 analog, 4F-benzoyl-TN14003, inhibits the migration and accumulation of rheumatoid T cells through a specific binding to CXCR4 in competition with CXCL12. This compound interfered with cellular and humoral immune responses in experimental arthritis models in mice, and showed inhibitory effects against the CIA development at levels comparable to, or above those of known drugs. Since T140 is an inverse agonist, which has no CXCL12-like agonistic activity [29], it and its analogs have the potential of becoming promising agents for RA chemotherapy as well as for AIDS and cancer chemotherapy.

Acknowledgements: This work was supported in part by a 21st Century COE Program "Knowledge Information Infrastructure for Genome Science", a Grant-in-Aid for Scientific Research from the Ministry of Education, Culture, Sports, Science and Technology, Japan and a Health and Labour Sciences Research Grant on Health Sciences focusing on Drug Innovation. The authors wish to thank Prof. Scott McN. Sieburth, Department of Chemistry, Temple University, PA, USA for proofreading the manuscript and providing useful comments.

References

[1] Nanki, T. and Lipsky, P.E. (2000) Arthritis Res. 2, 415–423.
[2] Nanki, T., Hayashida, K., El-Gabalawy, H.S., Suson, S., Shi, K., Girschick, H.J., Yavuz, S. and Lipsky, P.E. (2000) J. Immunol. 165, 6590–6598.
[3] Nagasawa, T., Kikutani, H. and Kishimoto, T. (1994) Proc. Natl. Acad. Sci. USA 91, 2305–2309.
[4] Bleul, C.C., Farzan, M., Choe, H., Parolin, C., Clark-Lewis, I., Sodroski, J. and Springer, T.A. (1996) Nature 382, 829–833.
[5] Oberlin, E., Amara, A., Bachelerie, F., Bessia, C., Virelizier, J.-L., Arenzana-Seisdedos, F., Schwartz, O., Heard, J.-M., Clark-Lewis, I., Legler, D.F., Loetscher, M., Baggiolini, M. and Moser, B. (1996) Nature 382, 833–835.
[6] Tashiro, K., Tada, H., Heilker, R., Shirozu, M., Nakano, T. and Honjo, T. (1993) Science 261, 600–603.
[7] Murakami, T., Nakajima, T., Koyanagi, Y., Tachibana, K., Fujii, N., Tamamura, H., Yoshida, N., Waki, M., Matsumoto, A., Yoshie, O., Kishimoto, T., Yamamoto, N. and Nagasawa, T. (1997) J. Exp. Med. 186, 1389–1393.
[8] Tamamura, H., Xu, Y., Hattori, T., Zhang, X., Arakaki, R., Kanbara, K., Omagari, A., Otaka, A., Ibuka, T., Yamamoto, N., Nakashima, H. and Fujii, N. (1998) Biochem. Biophys. Res. Commun. 253, 877–882.
[9] Fujii, N., Oishi, S., Hiramatsu, K., Araki, T., Ueda, S., Tamamura, H., Otaka, A., Kusano, S., Terakubo, S., Nakashima, H., Broach, J.A., Trent, J.O., Wang, Z. and Peiper, S.C. (2003) Angew. Chem. Int. Ed. Engl. 42, 3251–3253.
[10] Murakami, T., Zhang, T.-Y., Koyanagi, Y., Tanaka, Y., Kim, J., Suzuki, Y., Minoguchi, S., Tamamura, H., Waki, M., Matsumoto, A., Fujii, N., Shida, H., Hoxie, J., Peiper, S.C. and Yamamoto, N. (1999) J. Virol. 73, 7489–7496.
[11] Xu, Y., Tamamura, H., Arakaki, R., Nakashima, H., Zhang, X., Fujii, N., Uchiyama, T. and Hattori, T. (1999) AIDS Res. Hum. Retroviruses 15, 419–427.
[12] Tamamura, H., Hori, A., Kanzaki, N., Hiramatsu, K., Mizumoto, M., Nakashima, H., Yamamoto, N., Otaka, A. and Fujii, N. (2003) FEBS Lett. 550, 79–83.
[13] Koshiba, T., Hosotani, R., Miyamoto, Y., Ida, J., Tsuji, S., Nakamura, S., Kawaguchi, M., Kobayashi, H., Doi, R., Hori, T., Fujii, N. and Imamura, M. (2000) Clin. Cancer Res. 6, 3530–3535.
[14] Mori, T., Doi, R., Koizumi, M., Toyoda, E., Ito, D., Kami, K., Masui, T., Fujimoto, K., Tamamura, H., Hiramatsu, K., Fujii, N. and Imamura, M. (2004) Mol. Cancer Ther. 3, 29–37.
[15] Murakami, T., Maki, W., Cardones, A.R., Fang, H., Tun Kyi, A., Nestle, F.O. and Hwang, S.T. (2002) Cancer Res. 62, 7328–7334.
[16] Juarez, J., Bradstock, K.F., Gottlieb, D.J. and Bendall, L.J. (2003) Leukemia 17, 1294–1300.
[17] Burger, M., Glodek, A., Hartmann, T., Schmitt-Graft, A., Seilberstein, L.E., Fujii, N., Kipps, T.J. and Burger, J.A. (2003) Oncogene 22, 8093–8101.
[18] Tamamura, H., Hiramatsu, K., Mizumoto, M., Ueda, S., Kusano, S., Terakubo, S., Akamatsu, M., Yamamoto, N., Trent, J.O., Wang, Z., Peiper, S.C., Nakashima, H., Otaka, A. and Fujii, N. (2003) Org. Biomol. Chem. 1, 3663–3669.
[19] Tamamura, H., Hiramatsu, K., Kusano, S., Terakubo, S., Yamamoto, N., Trent, J.O., Wang, Z., Peiper, S.C., Nakashima, H., Otaka, A. and Fujii, N. (2003) Org. Biomol. Chem. 1, 3656–3662.
[20] Matthys, P., Hatse, S., Vermeire, K., Wuyts, A., Bridger, G., Henson, G.W., De Clercq, E., Billiau, A. and Schols, D. (2001) J. Immunol. 167, 4686–4692.
[21] Hart, F.D. and Huskisson, E.C. (1984) Drugs 24, 232–255.
[22] Arndt, U., Rittmeister, M. and Moller, B. (2003) Orthopade 32, 1095–1103.
[23] Magari, K., Nishigaki, F., Sasakawa, T., Ogawa, T., Miyata, S., Ohkubo, Y., Mutoh, S. and Goto, T. (2003) Inflamm. Res. 52, 524–529.
[24] Feng, Y., Broder, C.C., Kennedy, P.E. and Berger, E.A. (1996) Science 272, 872–877.
[25] Müller, A., Homey, B., Soto, H., Ge, N., Catron, D., Buchanan, M.E., McClanahan, T., Murphy, E., Yuan, W., Wagner, S.N., Barrera, J.L., Mohar, A., Verastegui, E. and Zlotnik, A. (2001) Nature 410, 50–56.
[26] Schols, D., Struyf, S., Van Damme, J., Este, J.A., Henson, G. and De Clercq, E. (1997) J. Exp. Med. 186, 1383–1388.
[27] Nagasawa, T., Nakajima, T., Tachibana, K., Iizasa, H., Bleul, C.C., Yoshie, O., Matsushima, K., Yoshida, N., Springer, T.A. and Kishimoto, T. (1996) Proc. Natl. Acad. Sci. USA 93, 14726–14729.
[28] Trent, J.O., Wang, Z., Murray, J.L., Shao, W., Tamamura, H., Fujii, N. and Peiper, S.C. (2003) J. Biol. Chem. 278, 47136–47144.
[29] Zhang, W., Navenot, J.M., Haribabu, B., Tamamura, H., Hiramatu, K., Omagari, A., Pei, G., Manfredi, J.P., Fujii, N., Broach, J.R. and Peiper, S.C. (2002) J. Biol. Chem. 277, 24515–24521.

Available online at www.sciencedirect.com
SCIENCE DIRECT
Biochemical and Biophysical Research Communications 318 (2004) 719–725
BBRC
www.elsevier.com/locate/ybbrc

HIV protease inhibitor nelfinavir inhibits replication of SARS-associated coronavirus

Norio Yamamoto,[a] Rongge Yang,[a] Yoshiyuki Yoshinaka,[a] Shinji Amari,[b] Tatsuya Nakano,[c] Jindrich Cinatl,[d] Holger Rabenau,[d] Hans Wilhelm Doerr,[d] Gerhard Hunsmann,[e] Akira Otaka,[f] Hirokazu Tamamura,[f] Nobutaka Fujii,[f] and Naoki Yamamoto[a,*]

[a] *Department of Molecular Virology, Bio-Response, Graduate School, Tokyo Medical and Dental University, 1-5-45 Yushima, Bunkyo-ku, Tokyo 113-8519, Japan*
[b] *Collaborative Research Center of Frontier Simulation Software for Industrial Science, Institute of Industrial Science, University of Tokyo, 4-6-1 Komaba, Meguro-ku, Tokyo 153-8505, Japan*
[c] *Division of Safety Information on Drug, Food, and Chemicals, National Institute of Health Sciences, 1-18-1 Kamiyoga, Setagaya-ku, Tokyo 158-8501, Japan*
[d] *Institute of Medical Virology, Frankfurt University Medical School, Paul-Ehrlich Str 40, D-60596 Frankfurt, Germany*
[e] *Department of Virology and Immunology, German Primate Center, Kellnerweg 4, D-37077 Gottingen, Germany*
[f] *Graduate School of Pharmaceutical Sciences, Kyoto University, Sakyo-ku, Kyoto 606-8501, Japan*

Received 7 April 2004
Available online 6 May 2004

Abstract

A novel coronavirus has been identified as an etiological agent of severe acute respiratory syndrome (SARS). To rapidly identify anti-SARS drugs available for clinical use, we screened a set of compounds that included antiviral drugs already in wide use. Here we report that the HIV-1 protease inhibitor, nelfinavir, strongly inhibited replication of the SARS coronavirus (SARS-CoV). Nelfinavir inhibited the cytopathic effect induced by SARS-CoV infection. Expression of viral antigens was much lower in infected cells treated with nelfinavir than in untreated infected cells. Quantitative RT-PCR analysis showed that nelfinavir could decrease the production of virions from Vero cells. Experiments with various timings of drug addition revealed that nelfinavir exerted its effect not at the entry step, but at the post-entry step of SARS-CoV infection. Our results suggest that nelfinavir should be examined clinically for the treatment of SARS and has potential as a good lead compound for designing anti-SARS drugs.

Keywords: Severe acute respiratory syndrome; Coronavirus; HIV protease inhibitor

Severe acute respiratory syndrome (SARS) is an emerging disease that was first reported in Guangdong Province, People's Republic of China, in November, 2002. Since then, SARS has spread to 32 countries and has resulted in more than 800 deaths from respiratory distress syndrome [1–3]. An overall estimate of case fatality reached 14–15% as reported by WHO [4] and the mortality rate in people older than 60 years could be as high as 43–55% [5].

Several groups, including the authors, isolated a novel coronavirus from SARS patients [2,6,7]. It has been shown that SARS-CoV satisfies Koch's postulates for causation—its consistent isolation from patients suffering from SARS, isolation of the virus and reproduction of disease in non-human primates after inoculation, and the presence of a specific antibody response against the virus in both SARS patients and artificially infected primates [8]. Now its etiological role in SARS is widely accepted.

The outbreak of SARS in several countries has led to the search for active antiviral compounds and vaccines for this disease [9]. Although the results of many clinical

* Corresponding author. Fax: +81-3-5803-0124.
E-mail address: yamamoto.mmb@tmd.ac.jp (N. Yamamoto).

0006-291X/$ - see front matter © 2004 Elsevier Inc. All rights reserved.
doi:10.1016/j.bbrc.2004.04.083

experiments have been reported, no consensus on treatment has been reached to date. Therapeutic protocols with steroids and ribavirin have been widely used empirically from the outset of the epidemic [10,11]. The use of steroids for SARS seemed beneficial, whenever they are appropriately applied. However, the optimal timing, dosage, and duration of treatment have not yet been determined. On the other hand, the administration of ribavirin did not apparently reduce either the rate of intratracheal intubation or that of mortality [12]. Moreover, significant toxicity, such as hemolytic anemia, has been attributed to ribavirin [13]. A few preliminary trials and in vitro data suggested the possibility of treating SARS with interferon [14–16]. Other agents including glycyrrhizin and convalescent plasma require further studies [17]. As is well established in the case of HIV-1 infection, the combination of antiviral drugs will make it possible to establish a better protocol for the treatment of SARS.

To identify anti-SARS drugs available for clinical use as rapidly as possible, we screened a set of compounds including antiviral drugs already in human clinical use. We found that nelfinavir, a widely used HIV-1 protease inhibitor, could inhibit SARS-CoV replication efficiently. Our results suggest that nelfinavir should be examined clinically for the treatment of SARS.

Materials and methods

Cell culture and virus. Vero E6 cells were maintained in Dulbecco's modified Eagle's medium supplemented with 10% FBS and glutamine–penicillin–streptomycin solution in 5% CO_2 in humidified air at 37 °C.

The FFM-1 strain of SARS-CoV was isolated from a SARS patient admitted to the Clinical Centre of Frankfurt University. This strain was used in all experiments to assess the antiviral activity of the drugs.

Compounds for screening. A set of compounds for screening consisted of 24 drugs as follows: nelfinavir, saquinavir, KNI-272, TYA5, TYB5, ritonavir, lopinavir, indinavir, 4F-benzoyl-TN14003, 4F-benzoyl-TE14011, TN14003, T140, TC14012, FC131, T22, SDF-1, vMIP-II, TAK-779, SC34, N36, T-20, glycyrrhizin, glycyrrhetic acid, and Cardran sulfate.

Cytopathic effect assay. SARS-CoV was inoculated into a monolayer of Vero E6 cells in 24-well plates at a multiplicity of infection (MOI) of 0.01. The plates were incubated at 37 °C in 5% CO_2 for 3 days and CPE in each well was observed.

Immunofluorescence assay. The Vero E6 cells in 24-well plates were infected with SARS-CoV at the MOI of 0.01. The infected cells were fixed with methanol 24 h after infection and incubated at room temperature for 1 h with diluted serum sample from a SARS patient. After washing with PBS, the cells were incubated with anti-human-IgG antibody conjugated with FITC for 30 min at room temperature. The cells were washed with PBS, mounted in buffered glycerol, cover-slipped, and viewed with a fluorescence microscope.

RNA extraction and real-time RT-PCR assay. SARS-CoV RNA in the culture supernatant was purified with ISOGEN (Nippongene) according to the manufacturer's protocol. For quantification of SARS-CoV ORF-1 RNA, we performed real-time RT-PCR with the primers and the probe as follows: ORF1-F, AGCTACGAGCACCAGACACC; ORF1-R, ACTTTGGGCATTCCCCTTT; ORF1-probe, TCGAAA TTAAGAGTGCCAAGAAATTTGACACTTT. The fluorescence intensity generated from the probe was detected by the ABI-7700 sequence detector system (Applied Biosystems).

MTT assay. Vero E6 cells in 96-well plates were infected with SARS-CoV at the MOI of 0.01. After 36 h of culture, cells were incubated for 4 h in the presence of 0.5 mg/ml of 3-(4,5-dimethylthiazol-2-yl)-2,5-diphenyl tetrazolium bromide (MTT). Formazan crystals were dissolved with 100 μL of 0.04 N HCl-isopropyl alcohol (acid isopropanol) and absorbance at 570 nm was measured with a reference wavelength of 655 nm.

Time-of-addition experiments. Drugs, including nelfinavir, were added to cultures of Vero E6 cells at the time of infection or 3 h after infection. Samples were processed for a quantitative RT-PCR assay and an immunofluorescence assay 24 h after infection. The cytopathic effect of infected cells was analyzed 36 h after infection.

Entry inhibition assay. Vero E6 cells were pretreated with each drug for 3 h, and SARS-CoV was inoculated at the MOI of 0.1. Cells and viruses were incubated for 3 h and washed with PBS three times. Subsequently, infected cells were lysed with ISOGEN (Nippongene) and RNA was purified according to the manufacturer's protocol. Extracted RNA samples were subjected to real-time RT-PCR analysis for quantification of SARS-CoV RNA as described above. As a loading control for normalization, 18S ribosomal RNA was quantified with the primers and the probe as follows: 18S-F, GTAACCCGTTGAACCCCATT; 18S-R, CCATCCAATCGGTAGTAGCG; and 18S-probe, TGCGTT GATTAAGTCCCTGCCCTTTGTA.

Results and discussion

Nelfinavir inhibited replication of SARS-CoV

We screened our chemical library and found that nelfinavir could inhibit SARS-CoV replication in Vero E6 cells. Nelfinavir clearly inhibited the cytopathic effect (CPE) induced by infection with SARS-CoV (Fig. 1A). We also examined the replication of SARS-CoV by immunofluorescence assay (IFA) with a serum sample from a patient with SARS. Expression of viral antigens was much lower in infected cells treated with nelfinavir than in untreated infected cells (Fig. 1B). Furthermore, we assessed the effect of nelfinavir on the production of virions. Nelfinavir significantly blocked the production of virions as revealed by quantitative RT-PCR (Fig. 2). By the use of MTT assay, we determined the concentration of the compound that reduced cell viability to 50% (CC_{50}), the concentration of the compound required for inhibition of CPE to 50% of the control value (EC_{50}), and the selectivity index (SI). Nelfinavir inhibited SARS-CoV replication at non-toxic doses with an approximate SI of 300, while the other inhibitors against HIV-1 protease (ritonavir, lopinavir, saquinavir, indinavir, TYA5, TYB5, and KNI-272) did not affect the replication of SARS-CoV (Table 1). These results revealed that nelfinavir is active in inhibiting SARS-CoV replication.

Nelfinavir inhibited SARS-CoV replication at the post-entry, but not the entry step

To disclose the step at which nelfinavir affects the virus life cycle, we performed time-of-addition experiments on the replication of SARS-CoV.

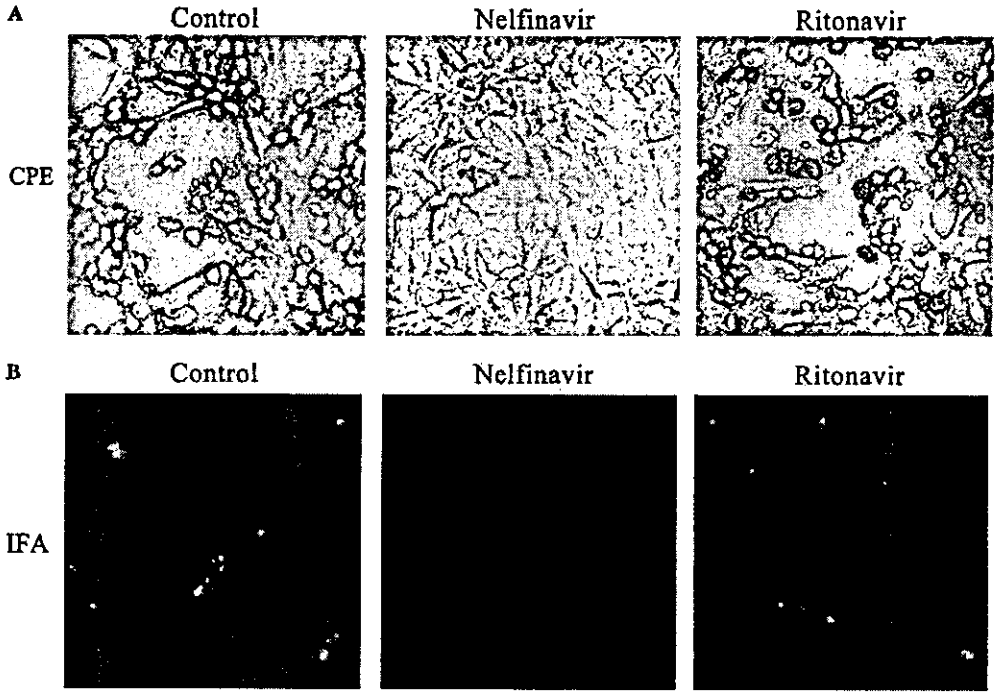

Fig. 1. Effect of nelfinavir on replication of SARS-CoV in Vero E6 cells. (A) Cytopathic effect (CPE) in Vero E6 cells. The cells were treated with phosphate-buffered saline (PBS) as a control, 10 μM nelfinavir, or 10 μM ritonavir for 3 h before infection. CPE was observed 36 h after infection. (B) Immunofluorescence assay (IFA) of infected cells treated with PBS, 10 μM nelfinavir, or 10 μM of ritonavir. Cells were fixed with methanol 24 h after infection and stained with serum samples from SARS patients.

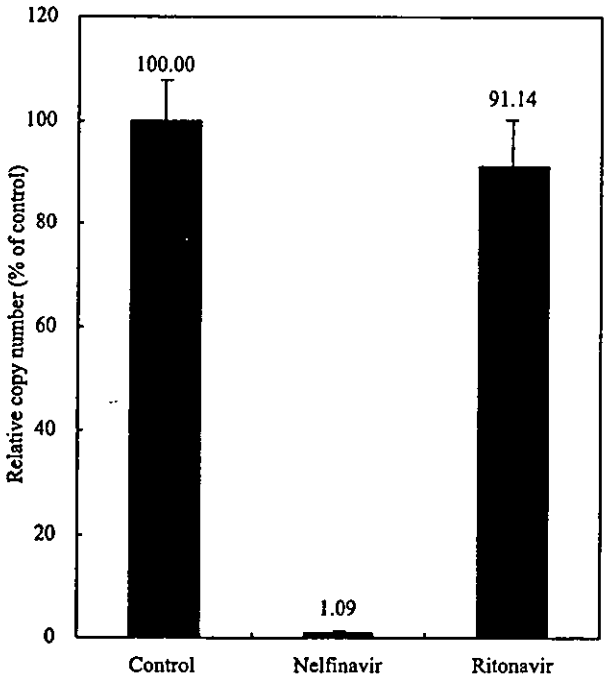

Fig. 2. Real-time RT-PCR for SARS-CoV RNA. Vero E6 cells had been treated with nelfinavir or ritonavir for 3 h before infection at the concentration of 10 μM. Instead of these drugs, PBS was added as a negative control. Viral RNA in the culture supernatant was collected 24 h after infection and quantified by the use of a fluorogenic probe. All samples were analyzed in triplicate.

Table 1
Activity of compounds against SARS-associated coronavirus in Vero cell cultures

Compound	EC_{50} (μM)	CC_{50} (μM)	Selectivity index
Nelfinavir	0.048 (0.024)	14.5 (2.75)	302.1
Saquinavir	NC	31.4 (7.82)	NC
KNI-272	NC	8.85 (2.05)	NC
TYA5	NC	16.3 (3.13)	NC
TYB5	NC	9.22 (2.25)	NC
Ritonavir	NC	13.8 (2.94)	NC
Lopinavir	NC	24.15 (5.01)	NC
Indinavir	NC	9.63 (3.11)	NC

NC, not calculable.

EC_{50}, effective concentration of compound needed to inhibit the cytopathic effect to 50% of control value.

CC_{50}, cytotoxic concentration of the compound that reduced cell viability to 50%.

Mean (standard error) of three assays was calculated for each drug.

Nelfinavir significantly inhibited SARS-CoV replication when used before infection (Figs. 1A and B and 2). When this drug was added at the time of infection or 3 h after infection, it was still able to block the CPE induced by SARS-CoV infection (Fig. 3A). Addition of nelfinavir at various timings inhibited the expression of viral antigens in Vero cells as shown by IFA (Fig. 3B). Nelfinavir blocked the production of virions when used to treat the cells at the time of infection or 3 h after infection (Fig. 4). The other protease inhibitors including ritonavir had no effect on replication of SARS-CoV